Technical Report Documentation Page

1. Report No.	2. Government Accession No.	3. Recipient's Catalog No.
SWUTC/09/476660-00007-1		

4. Title and Subtitle	5. Report Date
Improving the Sustainability of Asphalt Pavements through Developing a Predictive Model with Fundamental Material Properties	August 2009
	6. Performing Organization Code

7. Author(s)	8. Performing Organization Report No.
Rashid K. Abu Al-Rub, Eyad A. Masad, and Chien-Wei Huang	

9. Performing Organization Name and Address	10. Work Unit No. (TRAIS)
Texas Transportation Institute Zachry Department of Civil Engineering Texas A&M University College Station, TX 77843-3136	11. Contract or Grant No. DTRT07-G-0006

12. Sponsoring Organization Name and Address	13. Type of Report and Period Covered
Southwest Region University Transportation Center Texas Transportation Institute Texas A&M University System College Station, Texas 77843-3135	14. Sponsoring Agency Code

15. Supplementary Notes

Supported by a grant from the U.S. Department of Transportation, University Transportation Centers Program

16. Abstract

This study presents the numerical implementation and validation of general constitutive relationships for describing the nonlinear behavior of asphalt concrete mixes. These constitutive relationships incorporate nonlinear viscoelasticity and viscoplasticity to predict the recoverable and irrecoverable responses, respectively. The nonlinear viscoelastic deformation is modeled using Schapery's model; while the irrecoverable component is represented using Perzyna's viscoplasticity theory with an extended Drucker-Prager yield surface and plastic potential that is modified to capture the distinction between the compressive and extension behavior of asphalt mixes. The nonlinear viscoelastic and viscoplastic model is represented in a numerical formulation and implemented in a finite element (FE) code using a recursive-iterative algorithm for nonlinear viscoelasticity and the radial return algorithm for viscoplasticity. Then, the model is used to analyze the nonlinear viscoelastic and viscoplastic behavior of asphalt mixtures subjected to single creep recovery tests at different stress levels and temperatures. This experimental analysis includes the separation of the viscoelastic and viscoplastic strain components. Based on this separation, a systematic procedure is presented for the identification of the material parameters associated with the nonlinear viscoelastic and viscoplastic constitutive equations. Finally, the model is applied and verified against a set of creep-recovery tests on hot mix asphalt at different stress levels and temperatures.

17. Key Words	18. Distribution Statement
Mechanistic Model; Viscoelasticity; Viscoplasticity; Damage Mechanics; Hot Mix Asphalt; Finite Element; Creep-Recovery	No restrictions. This document is available to the public through NTIS: National Technical Information Service 5285 Port Royal Road Springfield, Virginia 22161

19. Security Classification (of this report)	20. Security Classification (of this page)	21. No. of Pages	22. Price
Unclassified.	Unclassified.	59	

Improving the Sustainability of Asphalt Pavements through Developing a Predictive Model with Fundamental Material Properties

by

Rashid K. Abu Al-Rub
Zachry Department of Civil Engineering

Eyad A. Masad
Zachry Department of Civil Engineering

&

Chien-Wei Huang
Zachry Department of Civil Engineering

Performing Agency:
Texas A&M University

Report # SWUTC/09/476660-00007-1

Sponsored by the
Southwest Region University Transportation Center
Texas Transportation Institute
Texas A&M University System
College Station, Texas 77843-3135

August 2009

Disclaimer

The contents of this report reflect the views of the authors, who are responsible for the facts and the accuracy of the information presented herein. This document is disseminated under the sponsorship of the Department of Transportation, University Transportation Centers Program in the interest of information exchange. The U.S. Government assumes no liability for the contents or use thereof.

Acknowledgment

The authors recognize that support for this research was provided by a grant from the U.S. Department of Transportation, University Centers Program to the Southwest Region University Transportation Center.

Abstract

This study presents the numerical implementation and validation of general constitutive relationships for describing the nonlinear behavior of asphalt concrete mixes. These constitutive relationships incorporate nonlinear viscoelasticity and viscoplasticity to predict the recoverable and irrecoverable responses, respectively. The nonlinear viscoelastic deformation is modeled using Schapery's model; while the irrecoverable component is represented using Perzyna's viscoplasticity theory with an extended Drucker-Prager yield surface and plastic potential that is modified to capture the distinction between the compressive and extension behavior of asphalt mixes. The nonlinear viscoelastic and viscoplastic model is represented in a numerical formulation and implemented in a finite element (FE) code using a recursive-iterative algorithm for nonlinear viscoelasticity and the radial return algorithm for viscoplasticity. Then, the model is used to analyze the nonlinear viscoelastic and viscoplastic behavior of asphalt mixtures subjected to single creep recovery tests at different stress levels and temperatures. This experimental analysis includes the separation of the viscoelastic and viscoplastic strain components. Based on this separation, a systematic procedure is presented for the identification of the material parameters associated with the nonlinear viscoelastic and viscoplastic constitutive equations. Finally, the model is applied and verified against a set of creep-recovery tests on hot mix asphalt at different stress levels and temperatures.

Executive Summary

Approximately 2.4 million miles of pavements in the United States have a hot mix asphalt (HMA) surface. HMA or asphalt concrete is a complex composite that comprises of mineral aggregates that are bound together using an asphalt binder. Asphalt binder is a by-product obtained from the distillation of naturally occurring crude oil. Mineral aggregates are obtained by quarrying and processing natural rocks. Mechanical properties of the composite asphalt concrete vary significantly depending on the proportioning (mix design), size and distribution of aggregates, and individual physio-chemical and mechanical properties of the constituent materials.

There has been significant emphasis in the past few years on warranties of the performance of asphalt pavements. However, one of the challenges in establishing these warranties by contractors and highway agencies is the lack of mechanistic models and fundamental material properties that can be used to predict and enhance performance. The majority of available performance models for asphalt pavements are empirical and they do not employ fundamental material properties. The researchers at Texas A&M University have worked in recent years on developing test protocols for measuring fundamental material properties of asphalt mixtures. There is a large need to integrate these properties in models that can be used by engineers to predict the performance of asphalt pavements. Therefore, the focus of this research is on integrating fundamental properties of constituent materials in a mechanistic model that can be used effectively in predicting the performance of an asphalt composite over a wide range of loading and environmental conditions. This objective fits well with the vision of the National Asphalt Roadmap developed by the Federal Highway Administration for asphalt pavements. This vision is stated as "Develop improved asphalt pavement technologies that ensure the continued delivery of safe and economical pavements to satisfy our Nation's needs".

This report presents a continuum model for simulating the nonlinear material behavior of asphalt mixes or asphalt concretes by incorporating nonlinear-viscoelasticity and viscoplasticity. The Schapery's single-integral nonlinear viscoelastic model describes the nonlinear viscoelastic response. The viscoplastic model of Perzyna-type models the time-dependent permanent deformations, using a Drucker–Prager-like yield surface which is modified to depend on the third deviatoric stress invariant, and to include more complex dependence on state of stress. A novel and systematic procedure for separating the recoverable (viscoelastic) and the unrecoverable

(viscoplastic) deformations from the total deformations is advocated in this study. This procedure allows one to identify the material constants associated with the viscoelastic constitutive equations independently of the material constants associated with the viscoplastic constitutive equations.

The nonlinear constitutive model is implemented numerically for three-dimensional, plane strain, and axisymmetric problems in the well-known commercial finite element code Abaqus through the user material subroutine UMAT. A series of simulations is presented to show the performance of the model and its implementation. Sensitivity studies are conducted for all model parameters and results due to various simulations corresponding to laboratory tests are presented. The model is verified against a limited number of laboratory creep-recovery tests for various stress levels, loading times, and temperatures. The model predicts well the experimental data.

Finally, work is currently underway at Texas A&M University for coupling the developed viscoelastic-viscoplastic model with a continuum damage mechanics-based model. Both damage due to mechanical loading and damage due to moisture conditioning will be incorporated into the current constitutive model. Moreover, the ability of the proposed model in predicting the overall fatigue performance of HMA layers under realistic loading conditions will be demonstrated through future studies by the current authors.

Table of Contents

List of Figures

List of Tables

1 Introduction

Roadways are designed to last until rehabilitation or replacement, and it is their degraded performance that dictates the design of pavements. It is, therefore, essential to be able to predict the degradation of an asphalt concrete through the development of a robust computational model that can effectively simulate the performance of an asphalt pavement under mechanical (e.g. traffic) and environmental (e.g. moisture, temperature) loading. Although all materials are heterogeneous, continuum models describe many materials' behavior in a way that allows computation of much more complex physical problems than otherwise feasible. To create a model capable of simulating whole sections of a roadway, this study will use a continuum approach to describe all facets of material behavior. Many past studies have characterized asphalt concrete and its phases using various models (some using continuum models and some using micromechanical approaches), and this section will describe several of these studies and models.

Experimental measurements have shown that the response of hot mix asphalt (HMA) contains recoverable (viscoelastic) and irrecoverable (viscoplastic) deformation components (e.g. Perl et al., 1983; Sides et al., 1985; Collop et al., 2003). The recoverable response can be characterized as a nonlinear viscoelastic. The nonlinearity is caused by localized high strain concentrations in the binder phase (Masad and Somadevan, 2002; Kose et al., 2000). The Schapery's single integral model has been used in the past to describe the effect of stress and strain level on the nonlinear viscoelastic behavior of viscoelastic materials (e.g. Christensen, 1968; Schapery, 1969; Schapery, 2000), and several numerical schemes of Schapery's theory have been developed and implemented using finite element (FE) to analyze the material viscoelastic response (e.g. Touati and Cederbaum, 1997, 1998; Haj-Ali and Muliana, 2004). Lee and Kim (1998) and Kim et al. (2007) have used a linear simplified form of the Schapery's viscoelastic model coupled with isotropic damage (Schapery, 1991) in order to simulate the nonlinear behavior of HMA. Sadd et al. (2004) employed the Schapery theory to represent the nonlinear viscoelastic behavior of asphalt mixes and implemented it in a finite element code using a recursive numerical scheme. Huang et al. (2007) implemented Schapery's nonlinear viscoelasticity model (Shapery, 1969) in a finite element code using the recursive-iterative numerical algorithm of Haj-Ali and Muliana (2004) to characterize the viscoelastic behavior of HMA subjected to shear loading at different temperatures and strain levels; however, without taking into consideration the viscoplastic response of HMA especially at high stress levels and high temperatures. Therefore, the focus of

the present study is on coupling nonlinear viscoelasticity and viscoplasticity for more accurate representation of the HMA mechanical behavior. Damage coupling will be considered in a future work.

Perzyna's viscoplasticity theory (Perzyna, 1971) has been used to describe the irrecoverable response of asphalt mixtures. Seibi et al. (2001) developed an elasto-viscoplastic constitutive model for HMA. This model used the Perzyna's theory of viscoplasticity with the Drucker-Prager yield surface to model the irrecoverable component. However, this model used an elastic model to represent the recoverable component which is not realistic for HMA especially at high stress levels and high temperatures. Lu and Wright (1998) developed a model that employed Perzyna's viscoplasticity theory to represent the irrecoverable component of HMA, and considered the recoverable response as elastic or linear viscoelastic. Masad et al. (2005) developed an elasto-viscoplastic model with non-associated flow rule based on conventional Drucker-Prager yield surface for HMA. This model modified Perzyna's viscoplasticity to include material anisotropy and isotropic damage but with no viscoelasticity. Masad et al. (2007) improved this model by employing an extended Drucker-Prager yield surface which accounted for the influence of stress state (extension versus compression) on material response, and implemented it in a finite element program. Nevertheless, surprisingly, those material constitutive models did not couple nonlinear viscoelasticity and viscoplasticity to predict the mechanical response of HMA which is shown in this paper to be crucial at high stress levels and high temperatures.

Therefore, the objectives of this research are to develop a general material constitutive model which integrates a nonlinear viscoelastic model with a viscoplastic model and to implement it into the finite element code Abaqus (2008) using a recursive-iterative numerical algorithm for viscoelasticity and return mapping algorithm for viscoplasticity. This study employs the Schapery's nonlinear viscoelastic model to represent the recoverable strain, whereas the viscoplastic strain is modeled using Perzyna's viscoplasticity theory. The model is used to analyze the experimental data on HMA mixtures subjected to creep-recovery tests at different temperatures and stress levels, and verify the ability of the model to analyze asphalt mixtures response under the boundary conditions of laboratory tests.

2 Viscoelastic-Viscoplastic Constitutive Model

Asphalt concretes are modeled as viscoelastic materials because the recoverable response of asphalt changes with time under constant load and varies for various load rates (Sides et al., 1985; Grenfell et al., 2009) and specifically as nonlinear viscoelastic materials because experiments have shown asphalt binder's response varies with load level and temperature nonlinearly (Cheung and Cebon, 1997; Airey et al., 2002a,b, 2004). It is readily observed that asphalt pavements in service frequently sustain load and recover deformations, so any accurate model for asphalt concrete must include viscoelasticity.

Asphalt concretes are modeled as viscoplastic materials because experiments and observation reveal that asphalt concretes undergo permanent deformation under high loads, and that the rate at which these permanent deformations accumulate varies with loading rate (Sides et al., 1985; Dessouky, 2005; Grenfell et al., 2008). Specifically, a modified Drucker–Prager yield surface and non-associated flow rule are used to conform to empirical observations of asphalt mix response (Dessouky, 2005; Masad et al. 2007). Because excessive permanent deformations may lead to unacceptable pavement performance, any accurate model for asphalt concrete must include viscoplasticity.

Assuming small strain deformations, the total deformation of an asphalt concrete mix subjected to an applied stress can be decomposed into a recoverable component (i.e. viscoelastic) and an irrecoverable (i.e. viscoplastic) component such that:

$$\varepsilon_{ij} = \varepsilon_{ij}^{nve} + \varepsilon_{ij}^{vp} \tag{1}$$

where ε_{ij} is the total strain tensor, ε_{ij}^{nve} is the nonlinear viscoelastic strain tensor, and ε_{ij}^{vp} is the viscoplastic strain tensor.

2.1 Nonlinear viscoelastic model

This study employs the Schapery's nonlinear viscoelastic theory to model the recoverable component. The recoverable strain of Schapery integral form (1969) under an applied stress σ^{τ} is expressed as:

$$\varepsilon^{nve}(t) = g_0 D_0 \sigma^t + g_1 \int_0^t \Delta D\left(\psi^t - \psi^{\tau}\right) \frac{d\left(g_2 \sigma^{\tau}\right)}{d\tau} d\tau \tag{2}$$

where D_0 is the instantaneous elastic compliance, ΔD is the transient compliance, g_0, g_1, and g_2 are nonlinear parameters related to stress or strain level, and ψ^t is the reduced time which can be a function of stress/strain shift factor, temperature shift factor, and other environment shift factors and is given by:

$$\psi^t = \int_0^t \frac{d\xi}{a_T a_s a_e} \tag{3}$$

where a_T is the temperature shift factor, a_s is the strain or stress shift factor, and a_e is the environment shift factor. For numerical convenience, this study uses the Prony series to represent the transient compliance ΔD as follows:

$$\Delta D^{\psi^t} = \sum_{n=1}^{N} D_n \left(1 - \exp\left(-\lambda_n \psi^t\right)\right) \tag{4}$$

where D_n is the n^{th} coefficient of Prony series associated with the n^{th} retardation time λ_n, and N is the number of Prony series components. In the above equations, the superimposed t and τ designates the response at specific time.

The three-dimensional isotropic constitutive relations can be decoupled into deviatoric and volumetric parts presented as:

$$\varepsilon_{ij}^{nve} = \frac{1}{2G} S_{ij} + \frac{\sigma_{kk}}{9K} \delta_{ij} = \frac{1}{2} J S_{ij} + \frac{1}{3} B \sigma_{kk} \delta_{ij} \tag{5}$$

where G and K are the shear and bulk moduli, respectively, J and B are the shear and bulk compliances, respectively, S_{ij} is the deviatoric stress, and σ_{kk} is the volumetric stress. Applying the Schapery's integral constitutive model in Eq. (2), the deviatoric and volumetric strain components can be expressed, respectively, as follows (Lai and Bakker, 1996):

$$e_{ij}^{nve,t} = \frac{1}{2} g_0^t J_0 S_{ij}^t + \frac{1}{2} g_1^t \int_0^t \Delta J^{(\psi^t - \psi^\tau)} \frac{d(g_2^\tau S_{ij}^\tau)}{d\tau} d\tau \tag{6}$$

$$\varepsilon_{kk}^{nve,t} = \frac{1}{3} g_0^t B_0 \sigma_{kk}^t + \frac{1}{3} g_1^t \int_0^t \Delta B^{(\psi^t - \psi^\tau)} \frac{d(g_2^\tau \sigma_{kk}^\tau)}{d\tau} d\tau \tag{7}$$

where $e_{ij}^{nve,t}$ is the deviatoric strain tensor and $\varepsilon_{kk}^{nve,t}$ is the volumetric strain tensor. The material constants J_0 and B_0 are the instantaneous elastic shear and bulk compliances, respectively.

Assuming the Poisson's ratio υ to be time-independent, the deviatoric strain $e_{ij}^{nve,t}$ and volumetric strain $\varepsilon_{kk}^{nve,t}$ components can be expressed in terms of the hereditary integral formulation after substituting Eq. (4) as follows (Huang et al., 2007):

$$e_{ij}^{nve,t} = \frac{1}{2}\left[g_0^t J_0 + g_1^t g_2^t \sum_{n=1}^{N} J_n - g_1^t g_2^t \sum_{n=1}^{N} J_n \frac{1-\exp(-\lambda_n \Delta\psi^t)}{\lambda_n \Delta\psi^t} \right] S_{ij}^t - \frac{1}{2} g_1^t \sum_{n=1}^{N} J_n \left[\exp(-\lambda_n \Delta\psi^t) q_{ij,n}^{t-\Delta t} - g_2^{t-\Delta t} \frac{(1-\exp(-\lambda_n \Delta\psi^t))}{\lambda_n \Delta\psi^t} S_{ij}^{t-\Delta t} \right] \tag{8}$$

$$\varepsilon_{kk}^{nve,t} = \frac{1}{3}\left[g_0^t B_0 + g_1^t g_2^t \sum_{n=1}^{N} B_n - g_1^t g_2^t \sum_{n=1}^{N} B_n \frac{1-\exp(-\lambda_n \Delta\psi^t)}{\lambda_n \Delta\psi^t} \right] \sigma_{kk}^t - \frac{1}{3} g_1^t \sum_{n=1}^{N} B_n \left[\exp(-\lambda_n \Delta\psi^t) q_{kk,n}^{t-\Delta t} - g_2^{t-\Delta t} \frac{(1-\exp(-\lambda_n \Delta\psi^t))}{\lambda_n \Delta\psi^t} \sigma_{kk}^{t-\Delta t} \right] \tag{9}$$

2.2 Parametric study on the effect of viscoelastic material constants

This section presents the results of a parametric study of the viscoelastic nonlinear parameters. The results are from a series of simulations in Abaqus. The results are reported at one integration point subjected to uniaxial stress of 50kPa for 30s then allowed to recover for 30s. The material properties used in the simulations are presented in Table 1.

Table 1. Viscoelastic material parameters.

n	$\lambda_n (1/\mathrm{s})$	$J_n (1/\mathrm{kPa})$
1	1.0	1.15×10^{-6}
2	0.1	1.49×10^{-6}
3	0.01	3.17×10^{-6}
4	0.001	6.37×10^{-6}
5	0.0001	2.61×10^{-6}
6	0.00001	96.1×10^{-6}
J_0	—	0.675×10^{-6}

Figure 1 shows the strain response for varying the parameter g_0. Figure 2 shows the strain response for varying the parameters g_1 and g_2.

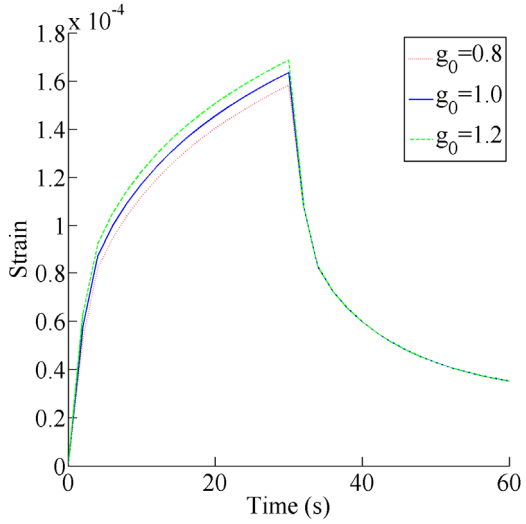

Figure 1. Effect of the viscoelastic nonlinear parameter g_0.

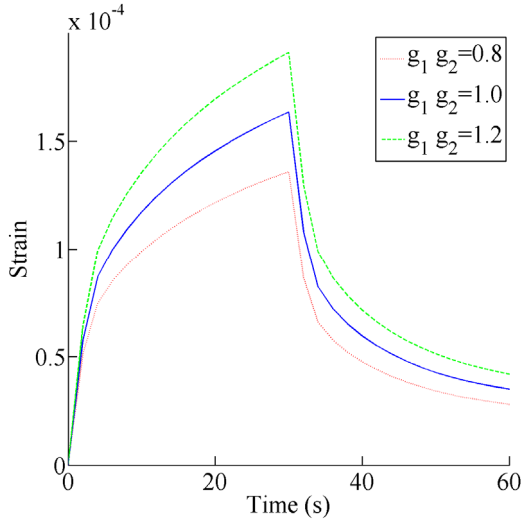

Figure 2. Effect of the viscoelastic nonlinear parameters g_1 and g_2.

2.3 Viscoplastic model

This study uses an Extended Drucker-Prager model with nonassociated flow rule to model the viscoplastic strain. From Eq. (1), the total strain rate $\dot{\varepsilon}_{ij}$ can be represented as:

$$\dot{\varepsilon}_{ij} = \dot{\varepsilon}_{ij}^{nve} + \dot{\varepsilon}_{ij}^{vp} \tag{10}$$

where $\dot{\varepsilon}_{ij}^{nve}$ is the viscoelastic strain rate and $\dot{\varepsilon}_{ij}^{vp}$ is the viscoplastic strain rate. This study uses Perzyna's model (Perzyna, 1971) to present the viscoplastic strain rate component as:

$$\dot{\varepsilon}_{ij}^{vp} = \Gamma\left\langle \phi(f) \right\rangle \frac{\partial g}{\partial \sigma_{ij}} \tag{11}$$

where Γ is the viscosity parameter, g is the viscoplastic potential energy function, and ϕ is the overstress function which is expressed in terms of the yield surface f. In Eq. (11), $\Gamma\langle\phi(f)\rangle$ is a positive scalar which determines the magnitude of viscoplastic strain rate $\dot{\varepsilon}_{ij}^{vp}$, and $\partial g/\partial\sigma_{ij}$ is a vector which dominants the direction of $\dot{\varepsilon}_{ij}^{vp}$. In addition, $\langle\bullet\rangle$ in Eq. (11) is the McCauley bracket such that the following expression for ϕ can be postulated:

$$\left\langle \phi(f) \right\rangle = \begin{cases} 0 & \phi(f) \le 0 \\ \left(\dfrac{f}{\sigma_y^0} \right)^N & \phi(f) > 0 \end{cases} \tag{12}$$

where σ_y^0 and N are material constants. Eqs. (11) and (12) indicate that the viscoplasticity takes place only when the overstress function exceeds zero. In order to consider the effects of confinement, deviatoric stress and dilative behavior of hot mix asphalt (HMA), this study employs Extended Drucker-Prager yield surface, which is presented in $I_1 - \tau$ plane as follows:

$$f = F\left(\sigma_{ij}\right) - \kappa\left(\varepsilon_e^{vp}\right) = \tau - \alpha I_1 - \kappa\left(\varepsilon_e^{vp}\right) \tag{13}$$

where α is a material parameter which is related to the material's internal friction. $\kappa\left(\varepsilon_e^{vp}\right)$ is an isotropic hardening function associated with the cohesive characteristics of the material and depends on the effective viscoplastic strain ε_e^{vp}, which is defined later. I_1 is the first stress invariant and τ is the deviatoric effective shear stress modified here to distinguish between the asphalt concrete behavior under compression and extension (not necessarily tension) loading condition, such that (Tashman et al., 2005):

$$\tau = \frac{\sqrt{J_2}}{2}\left[1 + \frac{1}{d} + \left(1 - \frac{1}{d} \right) \frac{J_3}{\sqrt{J_2^3}} \right] \tag{14}$$

where $J_2 = 3S_{ij}S_{ij}/2$ and $J_3 = (9/2)S_{ij}S_{jk}S_{ki}$ are the second and third deviatoric stress invariants, respectively, d is a material parameter which takes into account the distinction of asphalt

concrete behavior to compression and extension loading conditions. The range of d is from 0.778 to 1 (Masad et al., 2005). For uniaxial compression, the deviatoric effective shear stress $\tau = \sqrt{J_2}$; while $\tau = \frac{\sqrt{J_2}}{d}$ for uniaxial tension. A d less than 1 indicates that the material strength in compression is higher than the material strength in tension. If $d = 1$, the yield surface will become the Drucker-Prager yield surface.

Figure 3 shows the influence of stress path on the response using the modified Drucker-Prager yield surface, plotted in the $I_1 — \sqrt{J_2}$ plane. For a classical Drucker-Prager yield surface, $\alpha = \alpha'$ and $\kappa = \kappa'$, but the parameter d causes them to be different for the modified Drucker-Prager surface.

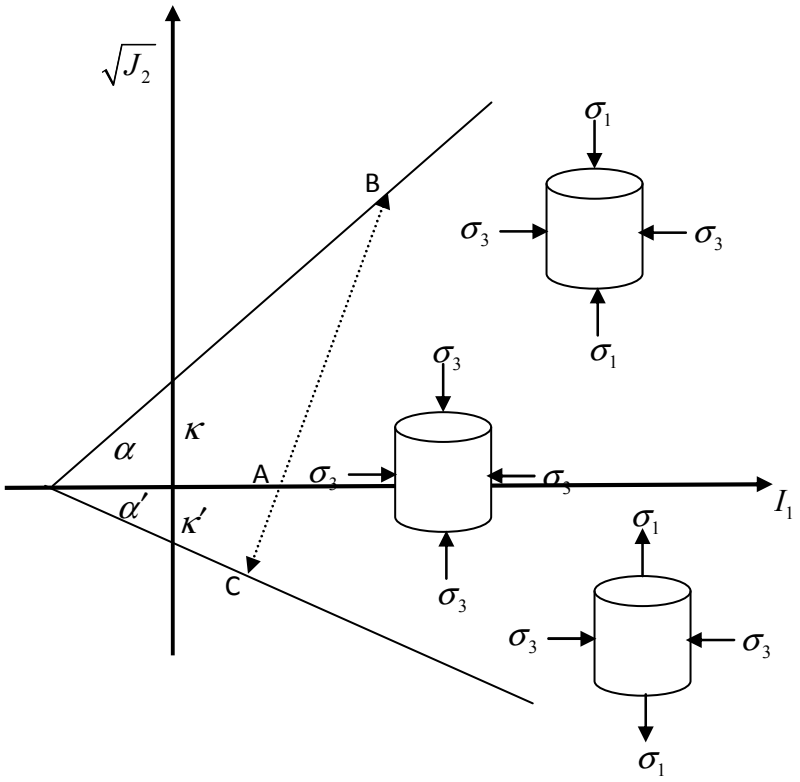

Figure 3. The influence of stress path for the modified Drucker-Prager yield surface.

The isotropic hardening function $\kappa\left(\varepsilon_e^{vp}\right)$ in Eq. (13) is expressed as an exponential function of the effective viscoplastic strain ε_e^{vp} following the work of Lemaitre and Chaboche (1990), such that:

$$\kappa = \kappa_0 + \kappa_1\left\{1-\exp\left(-\kappa_2\left(\varepsilon_e^{vp}\right)\right)\right\} \tag{15}$$

where κ_0, κ_1, and κ_2 are material parameters, which defines the initial yield stress, the saturated yield stress, and the strain hardening rate, respectively. The effective viscoplastic strain rate ε_e^{vp} is expressed as (Desouky, 2007):

$$\dot{\varepsilon}_e^{vp} = \frac{\left(1-\frac{\beta}{3}\right)}{\sqrt{\left(1-\frac{\beta}{3}\right)^2+2\left(\frac{1}{2}+\frac{\beta}{3}\right)^2}}\sqrt{\dot{\varepsilon}_{ij}^{vp}\dot{\varepsilon}_{ij}^{vp}} = \frac{1}{\sqrt{1+2\left(\frac{\frac{1}{2}+\frac{\beta}{3}}{1-\frac{\beta}{3}}\right)^2}}\sqrt{\dot{\varepsilon}_{ij}^{vp}\dot{\varepsilon}_{ij}^{vp}} \tag{16}$$

Several studies demonstrated that asphalt mixtures exhibit non-associated viscoplastic behavior which means that the direction of viscoplastic strain increment is not normal to the yield surface. The use of an associated flow rule (i.e. $g = f$) overestimates the dilation compared with experimental measurements (Masad et al., 2005, 2007). Hence, this study defines a viscoplastic potential function of a Drucker-Prager-type as in Eq. (13) by replacing α with a smaller parameter β, such that:

$$g = \tau - \beta I_1 \tag{17}$$

where β is a material parameter that describes the dilation or contraction behavior of the material.

From Eq. (17), $\partial g/\partial\sigma_{ij}$ in Eq. (11) can be expressed as:

$$\frac{\partial g}{\partial \sigma_{ij}} = \frac{\partial \tau}{\partial \sigma_{ij}} - \frac{1}{3}\beta\delta_{ij} \tag{18}$$

where δ_{ij} is the Kronecker delta and $\partial\tau/\partial\sigma_{ij}$ is given by:

$$\frac{\partial \tau}{\partial \sigma_{ij}} = \frac{1}{2}\left[\frac{\frac{\partial J_2}{\partial \sigma_{ij}}}{2\sqrt{J_2}}\left(1+\frac{1}{d}\right) + \left(\frac{\frac{\partial J_3}{\partial \sigma_{ij}} J_2 - \frac{\partial J_2}{\partial \sigma_{ij}} J_3}{J_2^2} \right)\left(1-\frac{1}{d}\right) \right] \tag{19}$$

where $\partial J_2 / \partial \sigma_{ij} = 3S_{ij}$ and $\partial J_3 / \partial \sigma_{ij} = \frac{27}{2} S_{ik} S_{kj} - 3J_2 \delta_{ij}$.

2.4 Parametric study on the effect of viscoplastic material constants

This section presents the results of a parametric study for all of the viscoplastic material parameters. The results are from a series of simulations in Abaqus. The results are reported at one integration point subjected to uniaxial strain at a constant strain rate $\dot{\varepsilon} = 0.0015$ for 60 seconds. In all cases uniaxial compression was simulated and in some cases it was deemed important to present results from simulations of uniaxial tension; when tensile simulation results are reported, they are plotted on the same axes as compression results with dashed lines.

All material parameters are held constant at the values from Table 1 (which may represent reasonable values for asphalt concrete) except the parameter being studied, which is varied with one larger and one smaller value. Presented here are nine figures plotting the stress in the direction the strain is applied versus the strain.

Table 2. Viscoplastic material parameters.

Property	Value
α	0.3
d	0.9
σ_y^0	35kPa
β	0.25
Γ	$5\times10^{-7}\,\mathrm{s}^{-1}$
N	2.0
κ_0	35kPa
κ_1	600kPa
κ_2	290

Figure 4 shows the effect of the yield surface parameter α, which controls the pressure sensitivity of the yield surface. For lower values of α, the tensile and compressive responses are more similar. Figure 5 shows the effect of the yield surface parameter d, which serves constrict the yield surface while the material undergoes extension, regardless of pressure. Notice that when the material is not being extended, d has no effect on the response. Figure 6 shows the effect of the yield surface parameter σ_y^0, which simply amplifies the yield surface.

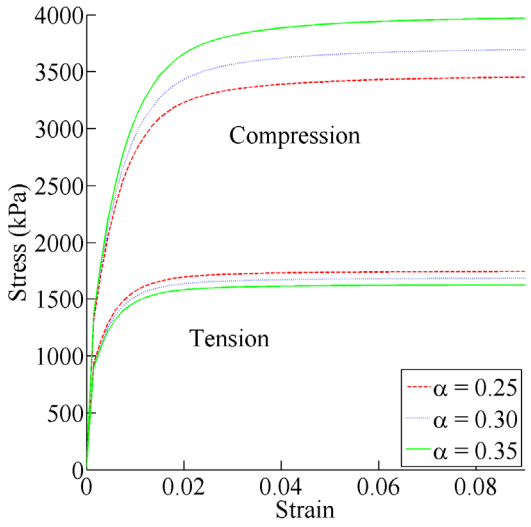

Figure 4. Effect of yield surface parameter α.

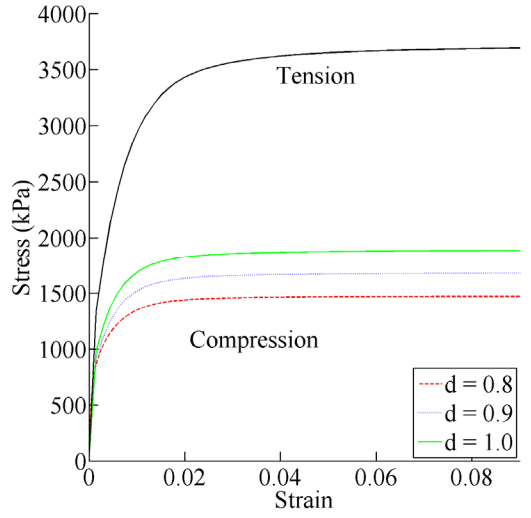

Figure 5. Effect of yield surface parameter d.

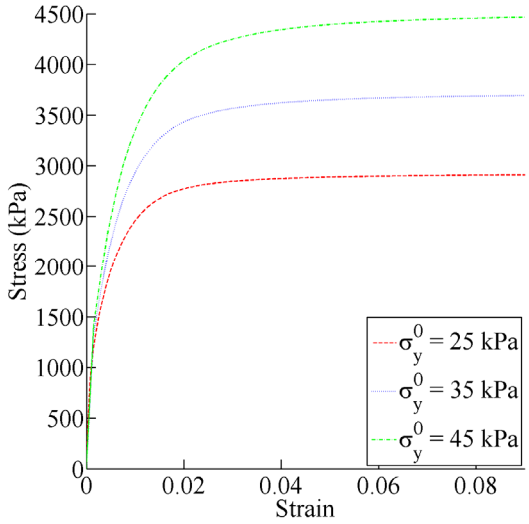

Figure 6. Effect of yield surface parameter σ_y^0.

Figure 7 shows the effect of the flow function parameter β, which makes the flow function pressure sensitive. As β increases, the plastic strain in compression decreases (i.e. the material is more stiff, as seen on the graph) and the plastic strain in tension increases (and hence the graph shows an more compliant response for higher values of β.) Figure 8 shows the effect of the flow function parameter Γ, which controls the amount of plastic strain based on the energy dissipated. Greater values of Γ correspond to more flow (and therefore smaller stresses). Figure 9 shows the effect of the flow function parameter N; greater values of N result in more flow.

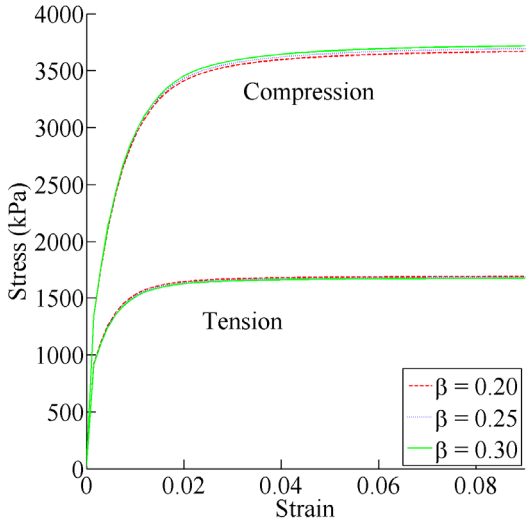

Figure 7. Effect of the viscoplastic potential energy parameter β.

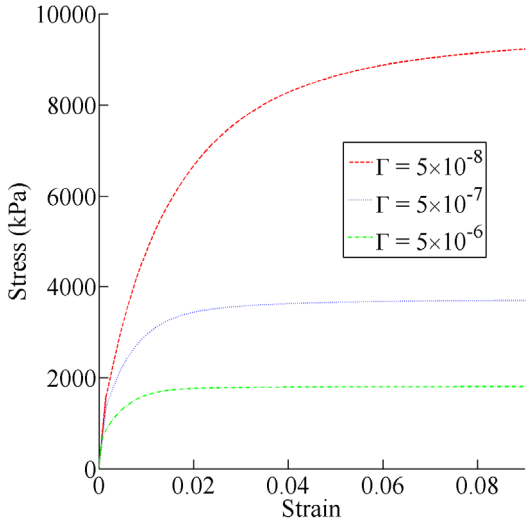

Figure 8. Effect of the viscoplastic potential energy parameter Γ.

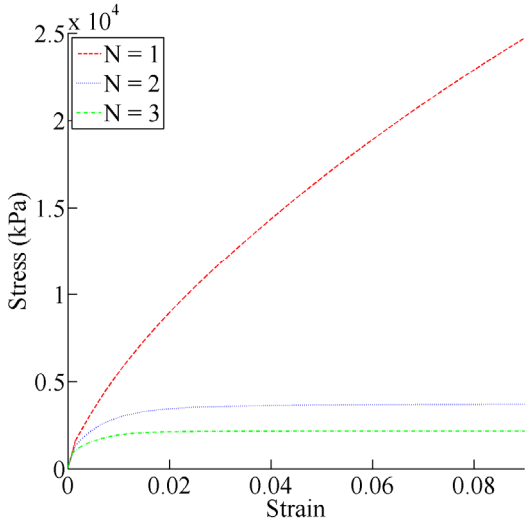

Figure 9. Effect of the viscoplastic potential energy parameter *N*.

Figures 10, 11, and 12 show the effect of the hardening function parameters κ_0, κ_1, and κ_2, and are best understood by understanding the hardening function κ, which is shown in Eq. (15). The value of the hardening function $\kappa(\dot{\varepsilon}_e^{vp})$ varies from κ_0 when $\dot{\varepsilon}_e^{vp} = 0$ (before viscoplasticity occurs) to $\kappa_0 + \kappa_1$ as $\dot{\varepsilon}_e^{vp} \to \infty$, and κ approaches the saturated value $\kappa_0 + \kappa_1$ more quickly as κ_2

increases. Figures 10 and 11 show the effects of κ_0 and κ_1 on the stress-strain behavior, a decrease in either decreases the value of the hardening function κ and results in a more compliant material. Figure 12 shows the effect of κ_2 on the stress-strain behavior, where the material yields more (has more flow) earlier for lower values of κ_2.

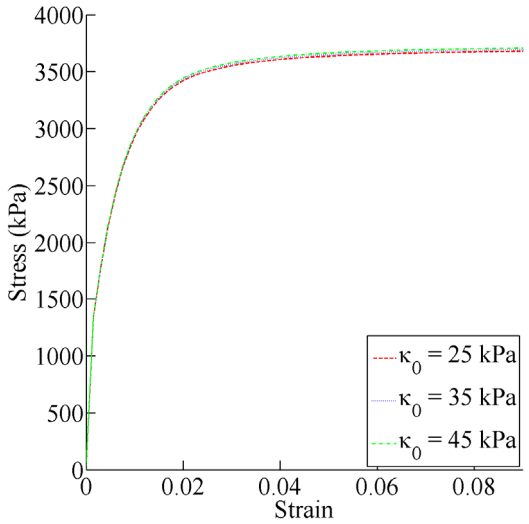

Figure 10. Effect of the hardening function parameter κ_0.

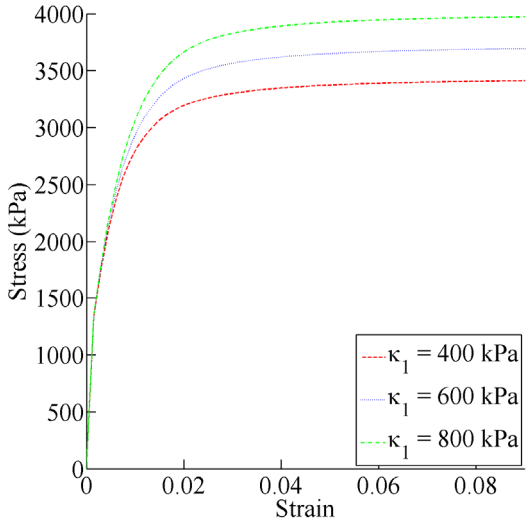

Figure 11. Effect of the hardening function parameter κ_1.

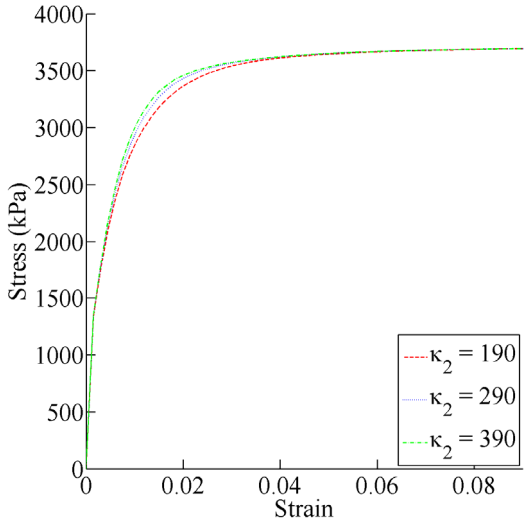

Figure 12. Effect of the hardening function parameter κ_2.

3 Numerical Implementation

In this section, the time discritization and numerical integration procedures for the presented nonlinear viscoelastic and viscoplastic model are presented. At the beginning of the step, by applying the given strain increment $\Delta\varepsilon_{ij} = \varepsilon_{ij}^{t+\Delta t} - \varepsilon_{ij}^{t}$ and knowing the values of the stress and internal variables from the previous step or time $t-\Delta t$, $(\square)^{t-\Delta t}$, the updated values at the end of the step or time t, $(\square)^{t}$, are obtained. Therefore, one can discretize the total strain in Eq. (1), the effective viscoplastic strain in Eq. (16), and the Cauchy stress tensor σ_{ij}, respectively, at the current time t as follows:

$$\varepsilon_{ij}^{t} = \varepsilon_{ij}^{nve,t} + \varepsilon_{ij}^{vp,t} = \varepsilon_{ij}^{t-\Delta t} + \Delta\varepsilon_{ij}^{t} = \varepsilon_{ij}^{nve,t-\Delta t} + \varepsilon_{ij}^{vp,t-\Delta t} + \Delta\varepsilon_{ij}^{nve,t} + \Delta\varepsilon_{ij}^{vp,t} \tag{1}$$

$$\varepsilon_{e}^{vp,t} = \varepsilon_{e}^{vp,t-\Delta t} + \Delta\varepsilon_{e}^{vp,t} \tag{2}$$

$$\sigma_{ij}^{t} = \sigma_{ij}^{t-\Delta t} + \Delta\sigma_{ij}^{t} \tag{3}$$

The viscoelastic bulk and deviatoric strain increments can be expressed from Eqs. (8) and (9) as follows (Huang et al., 2007):

$$\begin{aligned}\Delta e_{ij}^{nve,t} &= e_{ij}^{nve,t} - e_{ij}^{nve,t-\Delta t} \\ &= \overline{J}^{t} S_{ij}^{t} - \overline{J}^{t-\Delta t} S_{ij}^{t-\Delta t} - \frac{1}{2}\sum_{n=1}^{N} J_n \left[g_1^{t} \exp(-\lambda_n \Delta\psi^{t}) - g_1^{t-\Delta t} \right] q_{ij,n}^{t-\Delta t} - \\ &\quad \frac{1}{2} g_2^{t-\Delta t} \sum_{n=1}^{N} J_n \left\{ g_1^{t-\Delta t} \left[\frac{1-\exp(-\lambda_n \Delta\psi^{t-\Delta t})}{\lambda_n \Delta\psi^{t-\Delta t}} \right] - g_1^{t} \left[\frac{1-\exp(-\lambda_n \Delta\psi^{t})}{\lambda_n \Delta\psi^{t}} \right] \right\} S_{ij}^{t-\Delta t}\end{aligned} \tag{4}$$

$$\begin{aligned}\Delta\varepsilon_{kk}^{nve,t} &= \varepsilon_{kk}^{nve,t} - \varepsilon_{kk}^{nve,t-\Delta t} \\ &= \overline{B}^{t} \sigma_{kk}^{t} - \overline{B}^{t-\Delta t} \sigma_{kk}^{t-\Delta t} - \frac{1}{3}\sum_{n=1}^{N} B_n \left[g_1^{t} \exp(-\lambda_n \Delta\psi^{t}) - g_1^{t-\Delta t} \right] q_{kk,n}^{t-\Delta t} - \\ &\quad \frac{1}{3} g_2^{t-\Delta t} \sum_{n=1}^{N} B_n \left\{ g_1^{t-\Delta t} \left[\frac{1-\exp(-\lambda_n \Delta\psi^{t-\Delta t})}{\lambda_n \Delta\psi^{t-\Delta t}} \right] - g_1^{t} \left[\frac{1-\exp(-\lambda_n \Delta\psi^{t})}{\lambda_n \Delta\psi^{t}} \right] \right\} \sigma_{kk}^{t-\Delta t}\end{aligned} \tag{5}$$

where the variables $q_{ij,n}^{t-\Delta t}$ and $q_{kk,n}^{t-\Delta t}$ are the shear and volumetric hereditary integrals for every Prony series term n at previous time step $t-\Delta t$, respectively. The hereditary integrals are updated at the end of every converged time increment, which will be used for the next time increment and are expressed as follows (Haj-Ali and Muliana, 2004):

$$q_{ij,n}^{t} = \exp(-\lambda_n \Delta\psi^t) q_{ij,n}^{t-\Delta t} + (g_2^t S_{ij}^t - g_2^{t-\Delta t} S_{ij}^{t-\Delta t}) \frac{1-\exp(-\lambda_n \Delta\psi^t)}{\lambda_n \Delta\psi^t} \tag{6}$$

$$q_{kk,n}^{t} = \exp(-\lambda_n \Delta\psi^t) q_{kk,n}^{t-\Delta t} + (g_2^t \sigma_{kk}^t - g_2^{t-\Delta t} \sigma_{kk}^{t-\Delta t}) \frac{1-\exp(-\lambda_n \Delta\psi^t)}{\lambda_n \Delta\psi^t} \tag{7}$$

The increment of the viscoplastic strain in Eq. (11) can be rewritten as follows:

$$\Delta\varepsilon_{ij}^{vp,t} = \Gamma\left\langle \phi(f) \right\rangle \frac{\partial g}{\partial \sigma_{ij}} \Delta t = \Delta\gamma^{vp,t} \frac{\partial g}{\partial \sigma_{ij}} \tag{8}$$

where $\Delta\gamma^{vp,t}$ is the viscoplastic multiplier which is given by:

$$\Delta\gamma^{vp,t} = \Delta t \Gamma \left\langle \phi(f) \right\rangle = \Delta t \Gamma \left(\frac{f\left(\sigma_{ij}^t, \varepsilon_e^{vp,t}\right)}{\sigma_y^0} \right)^N \tag{9}$$

Substituting Eqs. (8) and (9) into (2), the effective viscoplastic strain increment can be shown as:

$$\varepsilon_e^{vp,t} = \varepsilon_e^{vp,t-\Delta t} + \Delta\varepsilon_e^{vp,t} = \varepsilon_e^{vp,t-\Delta t} + \frac{\Delta\gamma^{vp,t}}{\sqrt{1+2\left(\dfrac{\frac{1}{2}+\frac{\beta}{3}}{1-\frac{\beta}{3}}\right)^2}} \sqrt{\frac{\partial g}{\partial \sigma_{ij}} \frac{\partial g}{\partial \sigma_{ij}}} \tag{10}$$

The coupled nonlinear viscoelastic and viscoplastic algorithm starts at a trial stress, which is assumed to be viscoelastic and decomposed into deviatoric and volumetric components such that their increments can be expressed as follows [see Huang et al. (2007)]:

$$\Delta S_{ij}^{t,tr} = \frac{1}{\overline{J}^{t,tr}} \left\{ \Delta e_{ij}^t + \frac{1}{2} g_1^{t,tr} \sum_{n=1}^{N} J_n \left[\exp(-\lambda_n \Delta\psi^t) - 1 \right] q_{ij,n}^{t-\Delta t} \right\} \tag{11}$$

$$\Delta \sigma_{kk}^{t,tr} = \frac{1}{\overline{B}^{t,tr}} \left\{ \Delta \varepsilon_{kk}^t + \frac{1}{3} g_1^{t,tr} \sum_{n=1}^{N} B_n \left[\exp(-\lambda_n \Delta\psi^t) - 1 \right] q_{kk,n}^{t-\Delta t} \right\} \tag{12}$$

Once the trial stress exceeds the yield limit, the calculation of the viscoplastic strain increment is carried out; otherwise, the total stress and strain is viscoelastic.

According to Wang et al. (1997), one can define a consistency condition for rate-dependent plasticity (viscoplasticity) similar to rate-independent plasticity theory such that a dynamic (rate-dependent) yield surface, χ, can be expressed from Eqs. (11), (12), and (13) as follows:

$$\chi = \tau - \alpha I_1 - \kappa\left(\varepsilon_e^{vp}\right) - \sigma_y^0 \left(\frac{\dot{\gamma}^{vp}}{\Gamma} \right)^{1/N} \leq 0 \tag{13}$$

such that the above dynamic yield surface satisfies the Kuhn-Tucker loading-unloading conditions (consistency):

$$\chi \le 0; \quad \dot{\gamma}^{vp} \ge 0; \quad \dot{\gamma}^{vp}\chi = 0; \quad \dot{\chi} = 0 \tag{14}$$

A trial dynamic yield surface function χ^{tr} can be defined from Eq. (13) as:

$$\chi = \tau^{tr} - \alpha I_1^{tr} - \kappa\left(\left(\varepsilon_e^{vp,t-\Delta t}\right)\right) - \sigma_y^0\left(\frac{\Delta\gamma^{vp,t-\Delta t}}{\Delta t\Gamma}\right)^{1/N} \tag{15}$$

In order to calculate $\varepsilon_e^{vp,t}$, one can iteratively calculate $\Delta\gamma^{vp,t}$ through using the Newton-Raphson scheme. Once one obtains $\Delta\gamma^{vp,t}$, the viscoplastic strain increment $\Delta\varepsilon_{ij}^{vp}$ can be calculated from Eq. (8). In the Newton-Raphson scheme, the differential of χ with respect to $\Delta\gamma^{vp}$ is needed and can be expressed as follows:

$$\frac{\partial\chi}{\partial\Delta\gamma^{vp}} = -\frac{\partial\kappa}{\partial\Delta\varepsilon_e^{vp}}\frac{\partial\Delta\varepsilon_e^{vp}}{\partial\Delta\gamma^{vp}} - \frac{\sigma_y^0}{\Delta\gamma^{vp}N}\left(\frac{\Delta\gamma^{vp}}{\Delta t\Gamma}\right)^{\frac{1}{N}} \tag{16}$$

At the (k+1) iteration, the viscoplastic multiplier is calculated by:

$$\left(\Delta\gamma^{vp,t}\right)^{k+1} = \left(\Delta\gamma^{vp,t}\right)^{k} - \left[\left(\frac{\partial\chi}{\partial\Delta\gamma^{vp,t}}\right)^{k}\right]^{-1}\chi^{k} \tag{17}$$

Because both of the nonlinear viscoelastic and viscoplastic strain increments are functions of current stress, this study employs the recursive-iteration algorithm with the Newton-Raphson method to obtain the current stress and the updated values of the viscoelastic and viscoplastic strain increments by minimizing the residual strain defined as:

$$R_{ij}^t = \Delta\varepsilon_{ij}^{nve,t} + \Delta\varepsilon_{ij}^{vp,t} - \Delta\varepsilon_{ij}^t \tag{18}$$

This algorithm applies iterations at both the material and the structure levels to minimize the error; otherwise, very small increments are required. The stress increment at the (k+1) iteration is calculated by:

$$\left(\Delta\sigma_{ij}^t\right)^{k+1} = \left(\Delta\sigma_{ij}^t\right)^{k} - \left[\left(\frac{\partial R_{ij}^t}{\partial\sigma_{kl}^t}\right)^{k}\right]^{-1}\left(R_{kl}^t\right)^{k} \tag{19}$$

where the differential of R_{ij}^t gives the consistent tangent compliance, which can be derived as follows:

$$\frac{\partial R_{ij}^{t}}{\partial \sigma_{kl}} = \frac{\partial \Delta \varepsilon_{ij}^{nve,t}}{\partial \sigma_{kl}} + \frac{\partial \Delta \varepsilon_{ij}^{vp,t}}{\partial \sigma_{kl}} \tag{20}$$

where $\partial \Delta \varepsilon_{ij}^{nve} / \partial \sigma_{kl}$ is the nonlinear viscoelastic tangent compliance which is derived in Huang et al. (2007). Whereas, the viscoplastic tangent compliance is derived from Eqs. (8), (9), and (13), such that:

$$\begin{aligned} \frac{\partial \Delta \varepsilon_{ij}^{vp,t}}{\partial \sigma_{kl}} &= \frac{\partial g}{\partial \sigma_{ij}} \frac{\partial \Delta \gamma^{vp,t}}{\partial \sigma_{kl}} + \Delta \gamma^{vp,t} \frac{\partial^2 g}{\partial \sigma_{ij} \partial \sigma_{kl}} \\ &= \frac{\Delta t \Gamma N}{\sigma_y^0} \left(\frac{f}{\sigma_y^0} \right)^{N-1} \frac{\partial g}{\partial \sigma_{ij}} \frac{\partial f}{\partial \sigma_{kl}} + \Delta t \Gamma \left(\frac{f}{\sigma_y^0} \right)^{N} \frac{\partial^2 g}{\partial \sigma_{ij} \partial \sigma_{kl}} \end{aligned} \tag{21}$$

where $\partial^2 g / \partial \sigma_{ij} \partial \sigma_{kl}$ is given by:

$$\begin{aligned} \frac{\partial^2 \tau}{\partial \sigma_{ij} \partial \sigma_{kl}} = {} & 1.5 \left(\delta_{ik} \delta_{jl} - \frac{1}{3} \delta_{ij} \delta_{kl} \right) \left[\frac{1 + 1/d}{2\sqrt{J_2}} - \frac{J_3 \left(1 - 1/d \right)}{J_2^2} \right] \\ & + 1.5 S_{kl} \left[\frac{-\frac{\partial J_2}{\partial \sigma_{ij}} \left(1 + 1/d \right) J_2^{-1.5}}{4} + \left(1 - 1/d \right) \left(2 J_3 J_2^{-3} \frac{\partial J_2}{\partial \sigma_{ij}} - J_2^{-2} \frac{\partial J_3}{\partial \sigma_{ij}} \right) \right] \\ & + \frac{\left(1 - 1/d \right)}{2 J_2^2} \left[\frac{27 \left(\delta_{ik} S_{lj} + \delta_{jl} S_{ik} \right)}{2} - 9 \left(\delta_{kl} S_{ij} + \delta_{ij} S_{kl} \right) \right] \\ & - \left(\frac{27}{4} S_{km} S_{ml} - 1.5 J_2 S_{kl} \right) \left[\frac{\left(1 - 1/d \right) \frac{\partial J_2}{\partial \sigma_{ij}}}{J_2^2} \right] \end{aligned} \tag{22}$$

If the stress does not exceed the yield limit, the material compliance will only be the nonlinear viscoelastic compliance $\partial \Delta \varepsilon_{ij}^{nve} / \partial \sigma_{kl}$; otherwise, the material compliance will be a coupled nonlinear viscoelastic and viscoplastic one. The nonlinear viscoelastic and viscoplastic algorithm is shown in Figure 13. The flowchart of viscoplastic strain increment calculation using the Newton-Raphson method is shown in Figure 14.

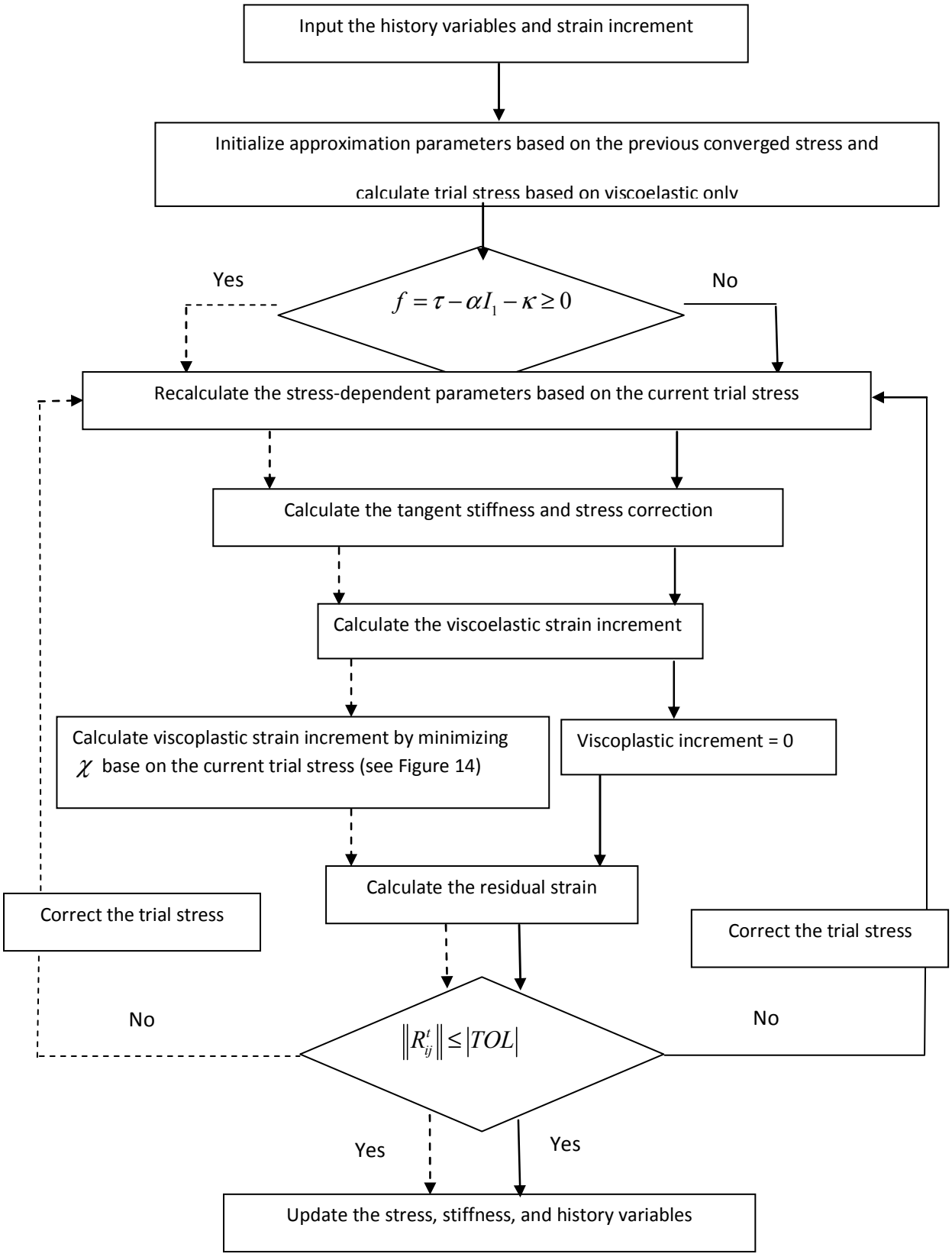

Figure 13. The flowchart of nonlinear viscoelastic and viscoplastic implementation.

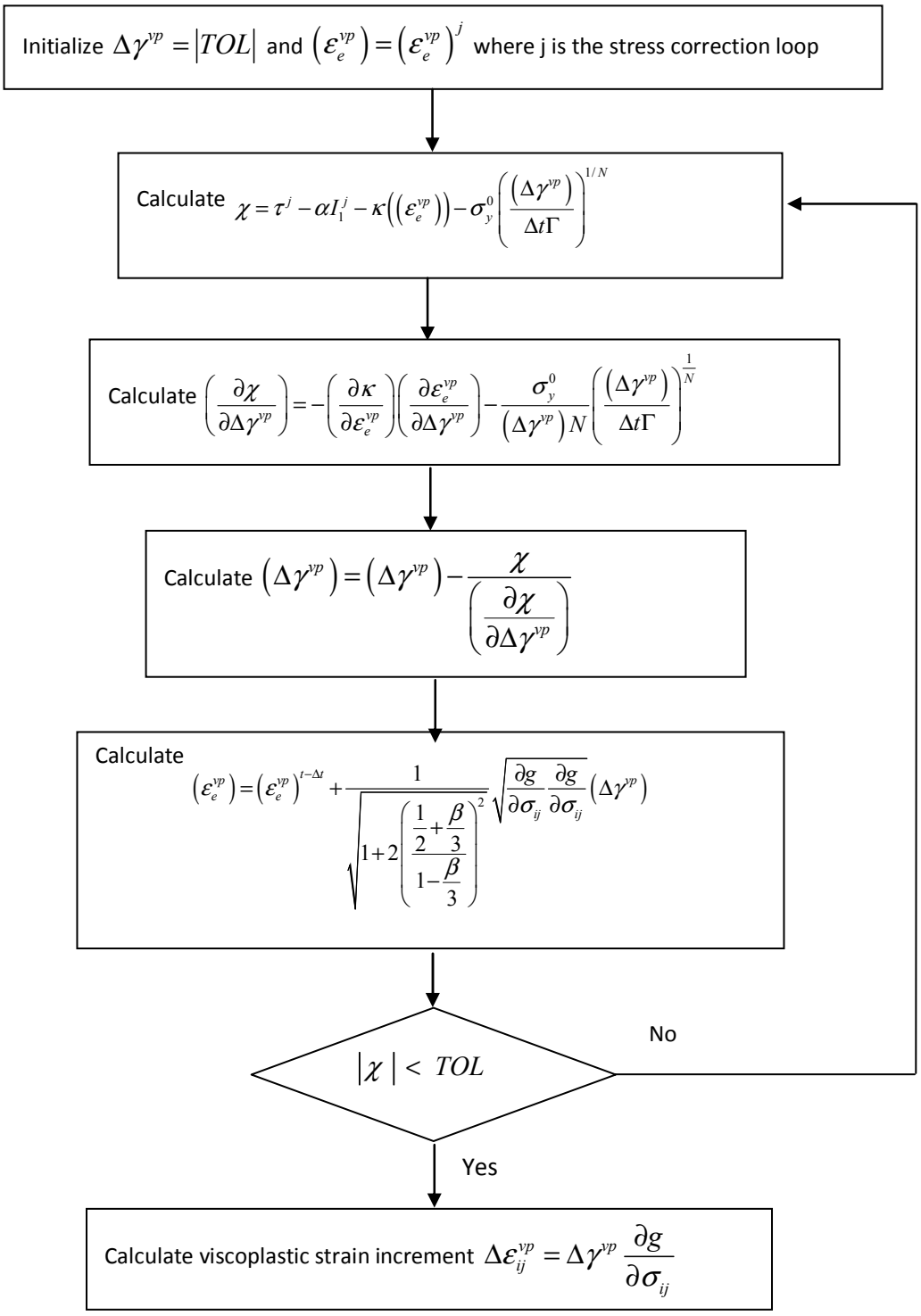

Figure 14. The flowchart of Newton-Raphson method for viscoplastic strain increments.

4 Calibration, Application, and Validation

In this Section, the presented computational constitutive model is calibration, validated, and applied to a set of experimental data on asphalt concrete mixes for different applied stress levels and temperatures. The asphalt mixture considered here for which experimental data is referred to as 10 mm Dense Bitumen Macadam (DBM) which is a continuously graded mixture with asphalt binder content of 5.5%. Granite aggregate and asphalt binder with a penetration grade of 70/100 is used in preparing the asphalt mixture. Cylindrical specimens with a diameter of 100mm and a height of 100mm were compacted using the gyratory compactor (Grenfell et al., 2009).

Single creep recovery tests are conducted over a range of temperatures and stress levels. The test conditions are summarized in Table 1. This test applies a constant step-loading and then remove the loading until the rate of recovered deformation during the relaxation period is approximately zero. The load is held for different loading times (LT) and the response is recorded for each LT as shown in Table 3. An example of experimental measurements at temperature 20 ^{o}C is shown in Figure 15. The details about the experimental results are given in the work of Grenfell et al. (2009).

Table 3. The summary of test conditions.

Temperature (^{o}C)	Stress Level (kPa) and loading times (LT) in sec	Reference stress level (kPa)
10	2000 (LT=400 and 600)	2000
	2500 (LT=300 and 350)	
20	1000 (LT=40, 210, 1517)	1000
	1500 (LT=30,150,420)	
40	500 (LT=130, 180)	500
	750 (LT=50)	

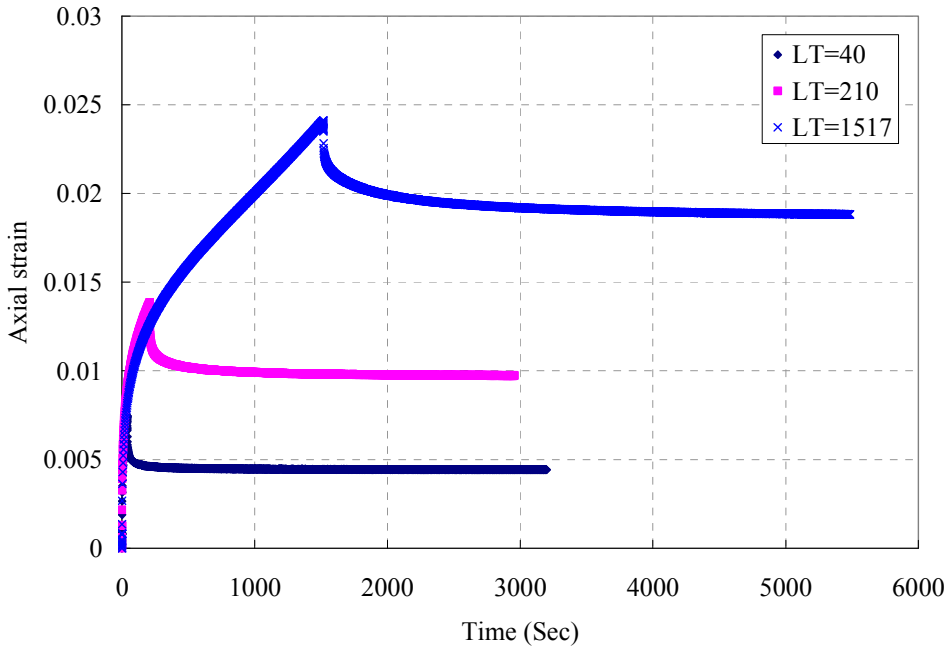

(a)

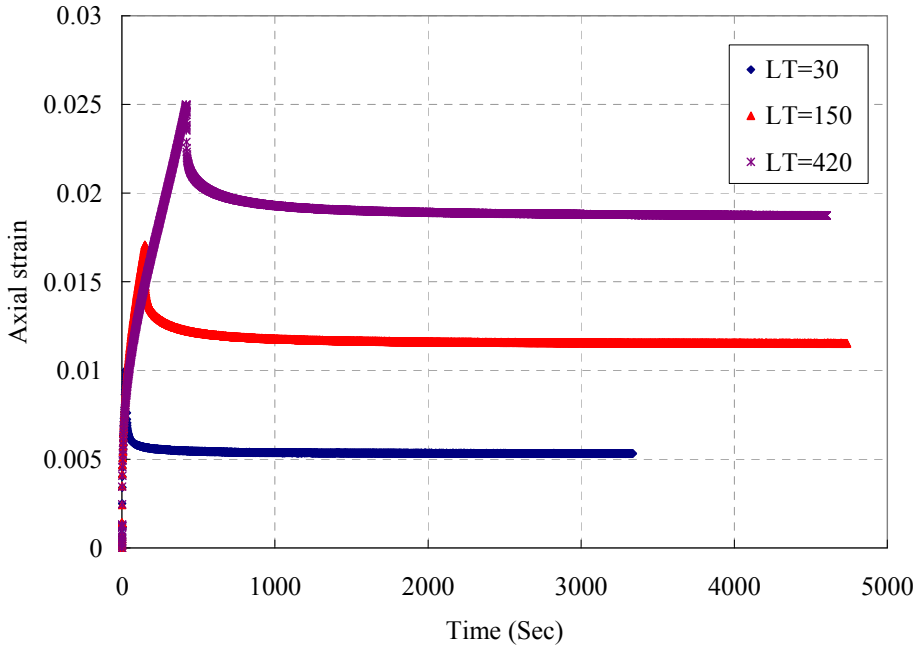

(b)

Figure 15. The experimental measurements at temperature 20^{o}C for stress levels: (a) 1000 kPa, and (b) 1500 kPa. LT indicates loading times in seconds.

4.1 Separation of recoverable and irrecoverable components

The first step of the following experimental analysis is to separate the recoverable (viscoelastic) and irrecoverable (viscoplastic) components. A schematic of a single creep-recovery test is shown in Figure 16 for a constant stress loading and unloading condition. Hence, one can express the creep and relaxation strains for a constant stress from Eqs. (1) and (2) as follows:

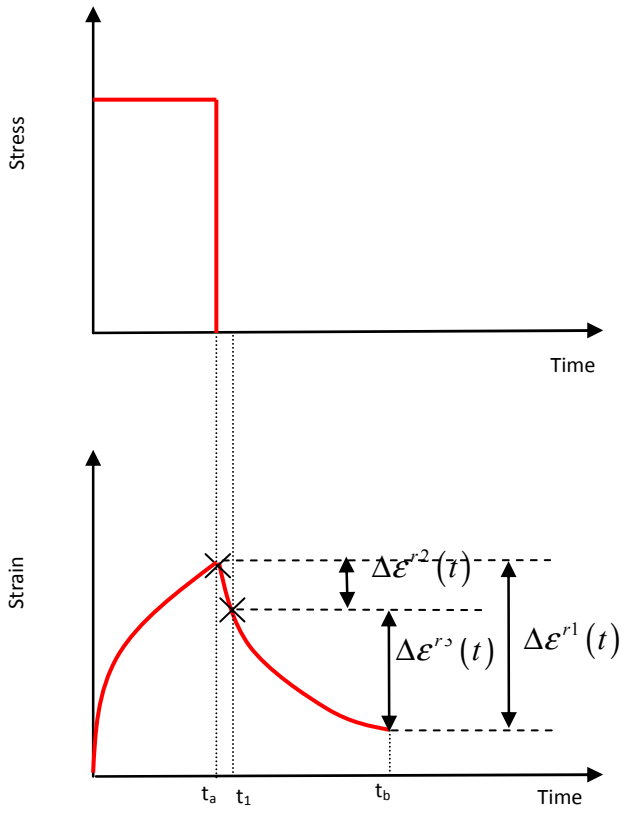

Figure 16. A schematic of single creep and recovery test.

$$\varepsilon^{c}(t)=\varepsilon^{rec}(t)+\varepsilon^{irrec}(t)=g_1 g_2\sigma\,\Delta D(t)+\varepsilon^{irrec}(t) \tag{23}$$

$$\varepsilon^{r}(t)=\varepsilon^{rec}(t)+\varepsilon^{irrec}(t_a)=\left[g_2\sigma\,\Delta D(t)-g_2\sigma\,\Delta D(t-t_a)\right]+\varepsilon^{irrec}(t_a) \tag{24}$$

where ε^{c} is the total creep strain, ε^{r} is the total relaxation strain, ε^{rec} is the recoverable strain, ε^{irrec} is the irrecoverable strain, t_a is the loading time shown in Figure 16. In this study, the entire recoverable strain component is assumed to be time-dependent such that one can set the instantaneous strain $g_0 D_0 \sigma = 0$. This is motivated by the experimental observations that show that it is very difficult to select the time at which the response could be considered to be

instantaneous (Saadeh et al., 2007). When the nonlinear parameters g_1 and g_2 are equal to unity, Eqs. (23) and (24) reduce to the linear vicoelastic case.

The first step of the analysis procedure is to obtain the Prony series coefficients D_n and λ_n in Eq. (4) from a linear viscoelastic response at low stress levels and low temperatures. However, in this study it is assumed that the recoverable response is linear viscoelastic ($g_1 = g_2 = 1$) at the lowest stress level of each considered temperature. The analysis employs the strain $\Delta\varepsilon^{r1}$ shown in Figure 16 which is the recovered strain between t_a and t_b in order to obtain the Prony series coefficients D_n and λ_n at the lowest stress level (linear viscoelastic case). The expression for $\Delta\varepsilon^{r1}(t)$ can be derived from Eqs. (23) and (24), such that:

$$\begin{aligned}\Delta\varepsilon^{r1}(t) &= \varepsilon^{c}(t_a) - \varepsilon^{r}(t) \\ &= \sigma \left\{ \begin{array}{l} \sum_{n=1}^{N} D_n \left[1 - \exp\left(-\lambda_n t_a\right)\right] - \\ \sum_{n=1}^{N} D_n \left[1 - \exp\left(-\lambda_n t\right)\right] + \sum_{n=1}^{N} D_n \left[1 - \exp\left(-\lambda_n (t - t_a)\right)\right] \end{array} \right\}\end{aligned} \tag{25}$$

Then, the Prony series coefficients are determined by minimizing the error between the measurements of $\Delta\varepsilon^{r1}(t)$ and Eq. (25). The values of D_n and λ_n at different temperatures are listed in Table 4. The nonlinear viscoelastic expressions in Eqs. (23) and (24) with D_n and λ_n shown in Table 4 can then be used to analyze the experimental measurements at higher stress levels in order to determine the nonlinear viscoelastic parameters g_1 and g_2. At the higher stress levels, the following expression for the recovered strain $\Delta\varepsilon^{r3}(t)$ from $t = t_1$ to $t = t_b$ (see Figure 16) can be derived from Eq. (24) and then used to determine the nonlinear parameter g_2, such that:

$$\begin{aligned}\Delta\varepsilon^{r3}(t) &= \varepsilon^{r}(t_1) - \varepsilon^{r}(t) \\ &= g_2\sigma \left\{ \begin{array}{l} \sum_{n=1}^{N} D_n \left[1 - \exp\left(-\lambda_n t_1\right)\right] + \sum_{n=1}^{N} D_n \left[1 - \exp\left(-\lambda_n (t_1 - t_a)\right)\right] - \\ \sum_{n=1}^{N} D_n \left[1 - \exp\left(-\lambda_n t\right)\right] + \sum_{n=1}^{N} D_n \left[1 - \exp\left(-\lambda_n (t - t_a)\right)\right] \end{array} \right\}\end{aligned} \tag{26}$$

Table 4. The Prony series coefficients.

n	λ_n (s^{-1})	Linear Viscoelastic Material Coefficients		
		Temp=10°C	20°C	40°C
		D_n (MPa^{-1})	D_n (MPa^{-1})	D_n (MPa^{-1})
1	10	7.81E-07	1.98E-07	3.98E-06
2	1	0.0	1.48E-06	0.0
3	0.1	5.42E-07	6.56E-07	1.55E-06
4	0.01	5.58E-07	1.43E-06	6.77E-07
5	0.001	1.62E-06	2.74E-06	6.05E-08

Once the nonlinear parameter g_2 is obtained, the expression for the recovered strain $\Delta\varepsilon^{r2}(t)$ which can be derived from Eqs. (23) and (24) is fitted to the experimental measurements from $t = t_a$ to $t = t_1$ (see Figure 16) in order to obtain the nonlinear parameter g_1, such that:

$$\Delta\varepsilon^{r2}(t) = \varepsilon^{c}(t_a) - \varepsilon^{r}(t) = \sigma \left\{ \begin{array}{l} g_1 g_2 \sum_{n=1}^{N} D_n \left[1 - \exp\left(-\lambda_n t_a\right)\right] - \\ g_2 \sum_{n=1}^{N} D_n \left[1 - \exp\left(-\lambda_n t\right)\right] + g_2 \sum_{n=1}^{N} D_n \left[1 - \exp\left(-\lambda_n (t - t_a)\right)\right] \end{array} \right\} \quad (27)$$

The nonlinear parameters at different temperatures are listed in Table 5. Once the Prony series coefficients (Table 4) and the nonlinear parameters (Table 5) are obtained, the nonlinear recoverable (viscoelastic) strain in Eqs. (23) and (24) can be calculated. Consequently, the irrecoverable (viscoplastic) strain can be obtained by subtracting the viscoelastic strain from the total strain. For example, the decoupled viscoelastic and viscoplastic responses are shown in Figure 17 for two stress levels at a temperature 20°C.

Table 5. The values of the nonlinear viscoelastic parameters at different temperatures.

Nonlinear viscoelastic parameters	Temperature (^{o}C)		
	10	20	40
g_1	0.908	1.194	0.576
g_2	1.017	0.837	1.920

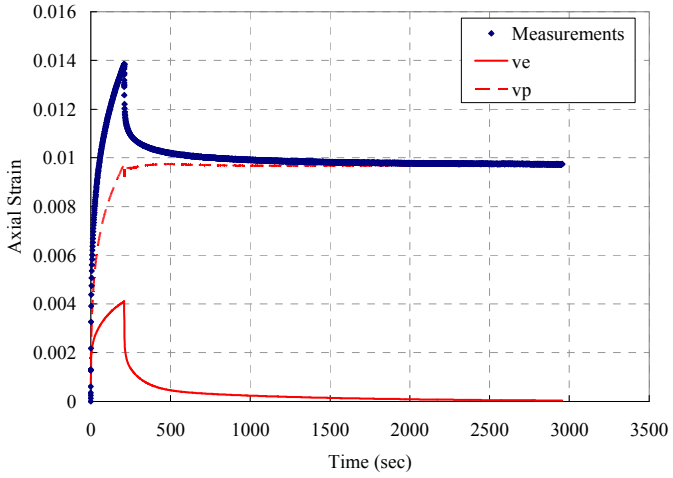

(a)

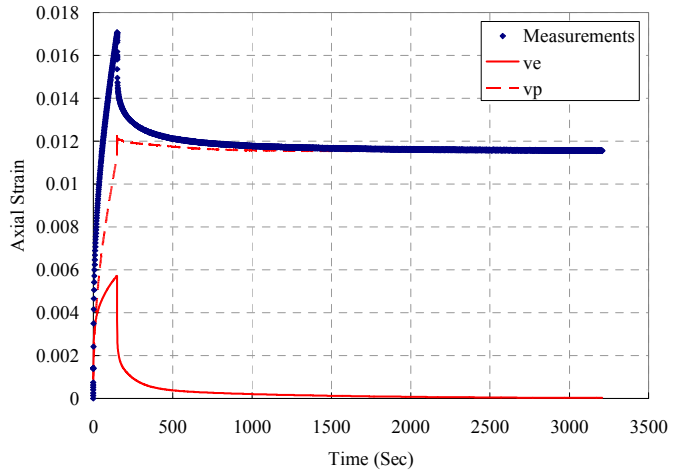

(b)

Figure 17. An example of separation of the viscoelastic and viscoplastic strains at temperature 20^{o}C for stress levels: (a) 1000 kPa, and (b) 1500 kPa.

4.2 Determination of the viscoplastic parameters

Once the viscoplastic strain is separated from the viscoelastic strain as shown in the previous section, one can then identify the material constants associated with the viscoplasticity equations as shown here. The dynamic yield surface in Eq. (13) for a uniaxial compression step-loading is expressed as:

$$\begin{aligned}\chi &= \sigma_1 - \alpha\frac{\sigma_1}{3} - \kappa\left(\varepsilon_e^{vp,t}\right) - \sigma_y^0\left(\frac{\Delta\gamma^{vp,t}}{\Delta t\Gamma}\right)^{1/N} \\ &= \sigma_1 - \alpha\frac{\sigma_1}{3} - \left[\kappa_0 + \kappa_1\left(1-\exp\left(-\kappa_2\varepsilon_e^{vp}\right)\right)\right] - \sigma_y^0\left(\frac{\Delta\gamma^{vp,t}}{\Delta t\Gamma}\right)^{1/N} \cong 0\end{aligned} \tag{28}$$

where σ_1 is the applied uniaxial compressive stress. By rearranging Eq. (28), one can write:

$$\frac{\Delta\gamma^{vp,t}}{\Delta t} = \Gamma\left[\frac{\left\{\sigma_1 - \alpha\frac{\sigma_1}{3} - \left[\kappa_0 + \kappa_1\left(1-\exp\left(-\kappa_2\varepsilon_e^{vp}\right)\right)\right]\right\}}{\sigma_y^0}\right]^N \tag{29}$$

where $\Delta\gamma^{vp,t}$ can be obtained from the separated $\Delta\varepsilon_1^{vp,t}$ from the experimental measurements for uniaxial compressive stress using the following expression obtained from Eq. (8), such that:

$$\Delta\gamma^{vp,t} = \frac{\Delta\varepsilon_1^{vp,t}}{\frac{\partial g}{\partial\sigma_1}} = \frac{\Delta\varepsilon_1^{vp,t}}{\left(1-\frac{\beta}{3}\right)} \tag{30}$$

where $\Delta\varepsilon_1^{vp,t}$ is the axial viscoplastic strain increment. Moreover, ε_e^{vp} can be calculated from Eq. (10) for uniaxial compression as:

$$\varepsilon_e^{vp} = \frac{1}{\sqrt{1+2\left(\frac{0.5+\beta/3}{1-\beta/3}\right)^2}}\sqrt{\left(\varepsilon_1^{vp}\right)^2 + 2\left(\varepsilon_2^{vp}\right)^2} \tag{31}$$

where ε_1^{vp} and ε_2^{vp} are the viscoplastic strains in the axial and radial directions, respectively. However, since the experimental measurements did not include ε_2^{vp}, this study calculates ε_2^{vp} from the following relation between the axial and radial viscoplastic strains. The relation between the axial and the radial viscoplastic strains for uniaxial compression can be determined from Eq. (11) as:

$$\frac{\varepsilon_2^{vp}}{\varepsilon_1^{vp}} = \frac{-\partial g / \partial \sigma_{22}}{\partial g / \partial \sigma_{11}} \Rightarrow \varepsilon_2^{vp} = \frac{0.5 + \beta/3}{1 - \beta/3} \varepsilon_1^{vp} \tag{32}$$

Once $\Delta\gamma^{vp,t}$ and ε_e^{vp} are calculated from the analyzed experimental viscoplastic strain data using Eqs. (30) and (31), the viscoplastic parameters Γ, N, κ_0, κ_1, and κ_2 can be obtained by minimizing the error between the measurements and Eq. (29).

Since the yield surface parameter α changes only slightly at small strain levels (Seibi et al., 2001), α is assumed here to be constant. The parameter β is also assumed to have a value less than α, because using $\alpha \geq \beta$ would result in higher dilation than is obtained from experimental measurements (Masad et al., 2007). However, β is assumed here to increase with temperature since asphalt mixtures dilates more as temperature increases. The assumed values of α and β are listed in Table 6.

Table 6. The values of the viscoplastic parameters at different temperatures.

Viscoplastic parameters	Temperature (^{o}C)		
	10	20	40
α	0.35	0.30	0.25
β	0.10	0.15	0.20
Γ	4.0E-4	5.0E-4	1.0E-2
N	3.63	3.63	3.63
κ_0	40	35	10
κ_1	930	610	550
κ_2	270	215	160

Furthermore, it is found that σ_y^0 is stress-dependent and follows $\sigma_y^0 = \sigma_1(1-\alpha/3)$ which is used to obtain the viscoplastic parameters such that Eq. (29) can be rewritten as follows:

$$\frac{\Delta\gamma^{vp,t}}{\Delta t} = \Gamma\left[1 - \frac{\left[\kappa_0 + \kappa_1\left(1-\exp\left(-\kappa_2\varepsilon_e^{vp}\right)\right)\right]}{\sigma_1 - \alpha\dfrac{\sigma_1}{3}}\right]^N \tag{33}$$

The advantages of the above analysis procedure are: (1) fitting the material response at different stress levels simultaneously; (2) normalizing the overstress function, which represents the distance between the current stress and the yield surface over a scale between 0 and 1, such that Γ is used then to determine the magnitude of viscoplastic increment; and (3) incorporating the applied stress effect within the dynamic yield surface. The fitting for both stress levels at a temperature 20 ^{o}C is shown in Figure 18, where the viscoplastic parameters at different temperatures are listed in Table 6.

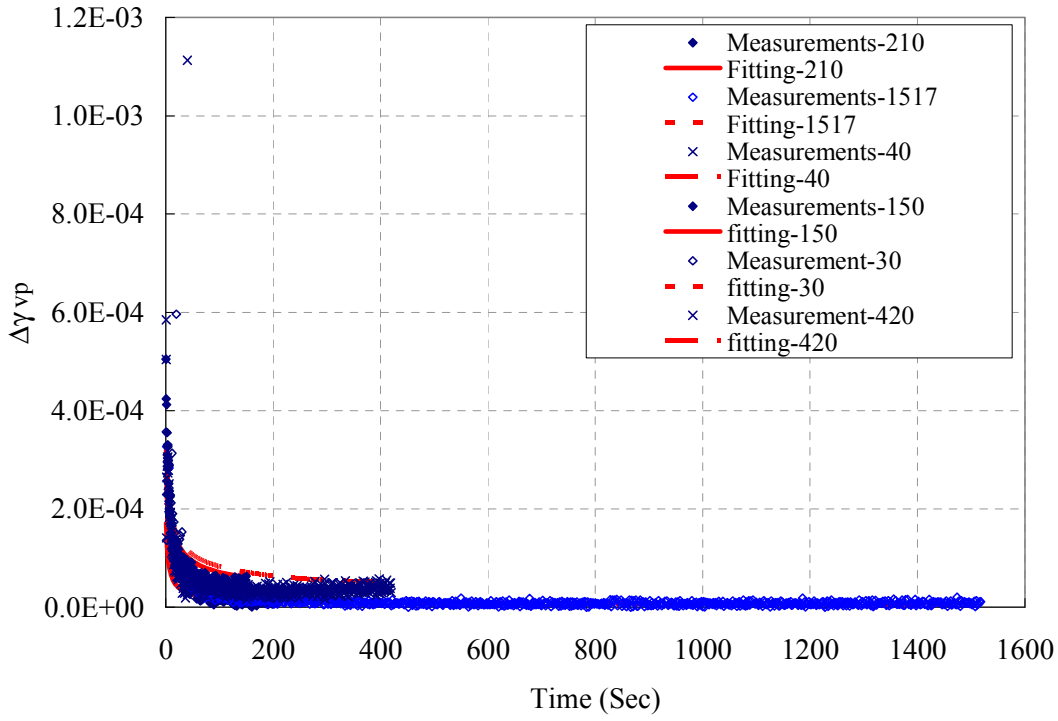

Figure 18. The viscoplastic fitting procedure of $\Delta\gamma^{vp}$ for different loading times (in seconds) and stress levels (in kPa) at temperature 20^{o}C.

4.3 Numerical predictions of experimental measurements

Once the viscoelastic material parameters (D_n, λ_n, g_1, and g_2) and the viscoplastic material parameters (Γ, N, σ_y^0, κ_0, κ_1, κ_2, α, and β) are determined, then the UMAT subroutine in the finite element code Abaqus (2008) is used to calculate the creep-recovery response and compare the results with the experimental measurements. The finite element model considered here is simply a three-dimensional single element (C3D8R) which is used to obtain the response due to creep-recovery loading. Figure 19 shows a comparison between the experimental data and the predictions for the total strain at a temperature 20 ^{o}C, where reasonable agreement is obtained. Figures 8 and 9 show comparisons of the measured and predicted viscoelastic and viscoplastic strains at a temperature 20 ^{o}C, respectively. Good predictions are obtained for the viscoplastic strain. Figures 10 and 11 show the comparison of total strain between experimental measurements and predictions at temperatures 10 ^{o}C and 40 ^{o}C, respectively, where again reasonable agreements are obtained. The predictions deviate from the experimental data for the cases (1) stress level=1500 kPa for LT=420 secs at temperature 20 ^{o}C, (2) stress level=2500 kPa for LT=300 secs at temperature 10 ^{o}C, and (3) stress level=500 kPa for LT=180 secs at temperature 40 ^{o}C. By looking at the experimental measurements of these cases (Figures 7 (b), 10 (b) and 11 (a)), the responses are deviant as compared with the other measurements at the same stress level and temperature. Generally, the creep response for different loading times should follow the same curve, which is not the case in these reported experiments. Hence, the FE predictions deviate from the measurements for these cases and it will be very difficult to get closer predictions of the creep-recovery experimental data. Therefore, more accurate and cleaner experimental data are desirable to fully validate the presented model, which is the scope of a current work by the authors.

Moreover, the FE model with the calibrated material parameters is used to analyze the material response at different temperatures. The simulated case involves a step-loading applying a stress level of 500 kPa for 180 secs. The comparison of the resulted material response is shown in Figure 12. This figure shows that increasing the temperature increases the total, viscoelastic, and viscoplastic strains, which is expected. Figure 13 shows the viscoelastic and viscoplastic parts of the total strain for different temperatures as compared to experimental data. This figure shows that increasing the temperature from 10 to 40 ^{o}C increases the viscoplastic portion from 60% to 70%, whereas the viscoelastic portion decreases from 40% to 30%.

Moreover, the percentage of the viscoelastic strain decreases with increasing the loading time; while the portion of viscoplastic strain increase with the loading time time. Also, the results indicate that the viscoplastic component dominates the material response at higher temperatures, whereas the viscoelastic component is more important at lower temperatures.

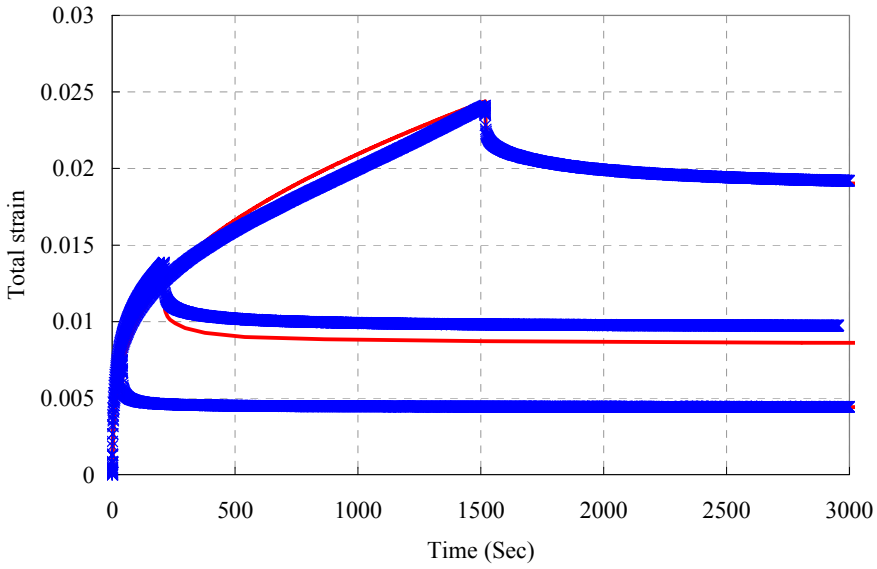

(a)

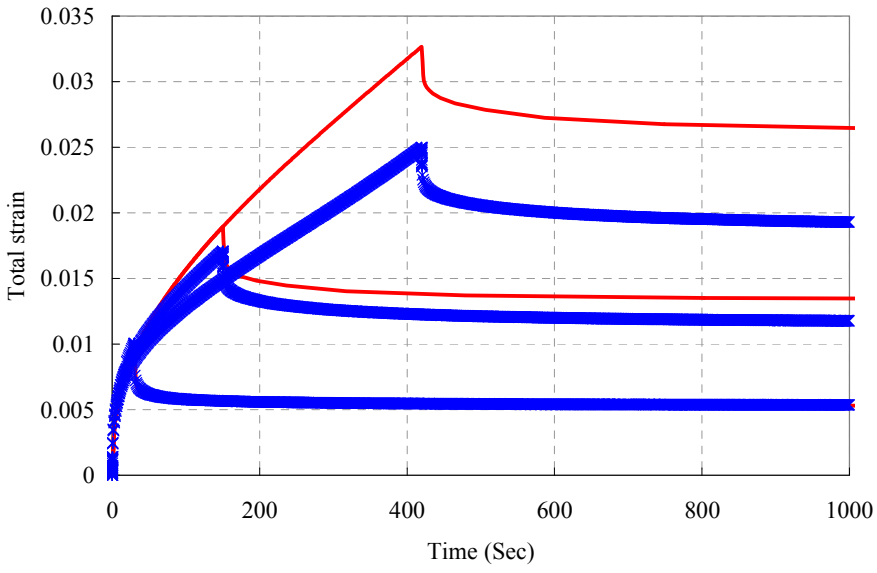

(b)

Figure 19. The comparison of total strain between measurements and model predictions at temperature 20°C for stress levels: (a) 1000 kPa and (b) 1500 kPa.

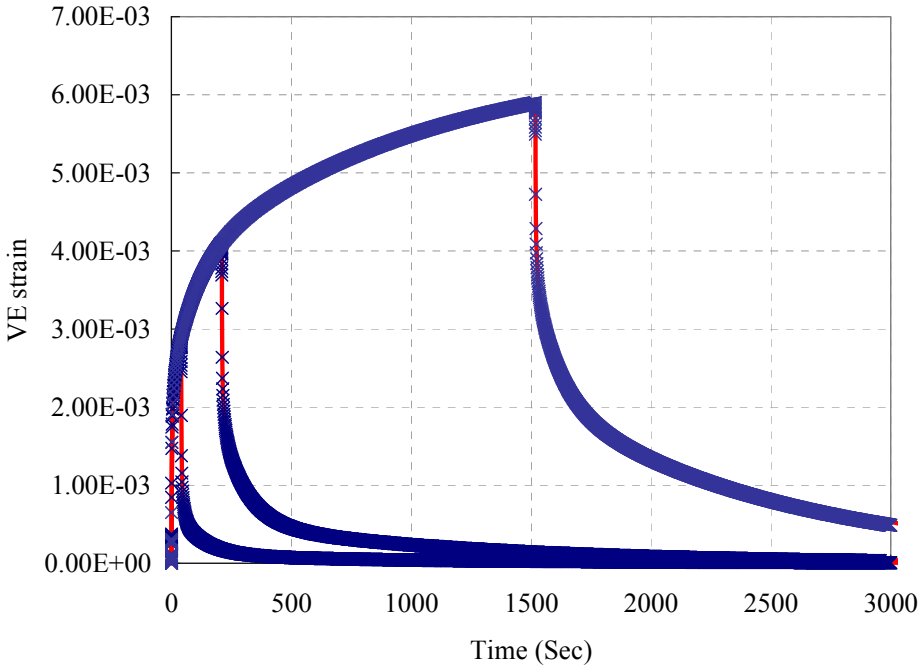

(a)

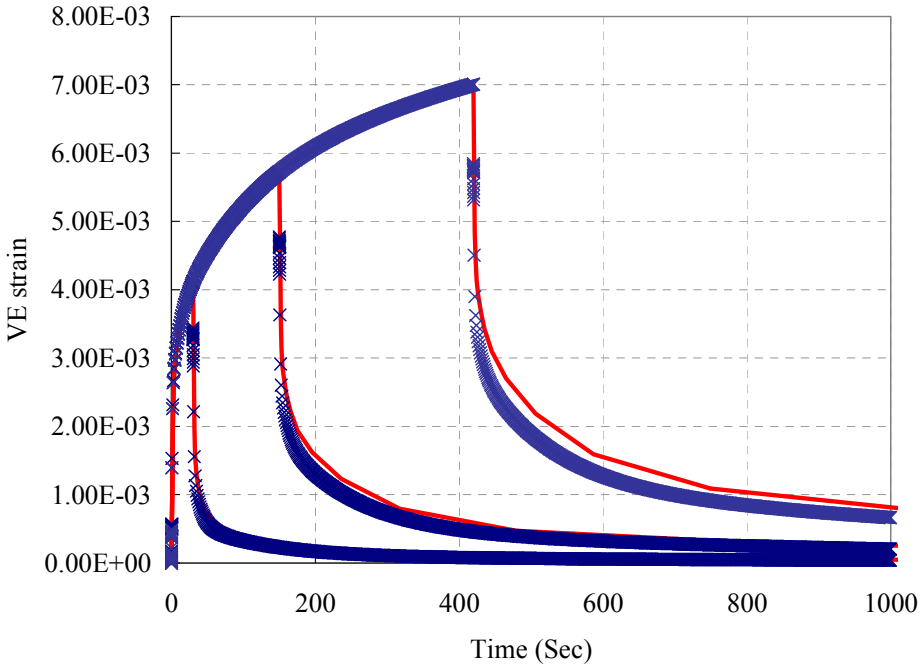

(b)

Figure 20. The comparison of viscoelastic strain between measurements and model predictions at temperature 20°C for stress levels: (a) 1000 kPa and (b) 1500 kPa.

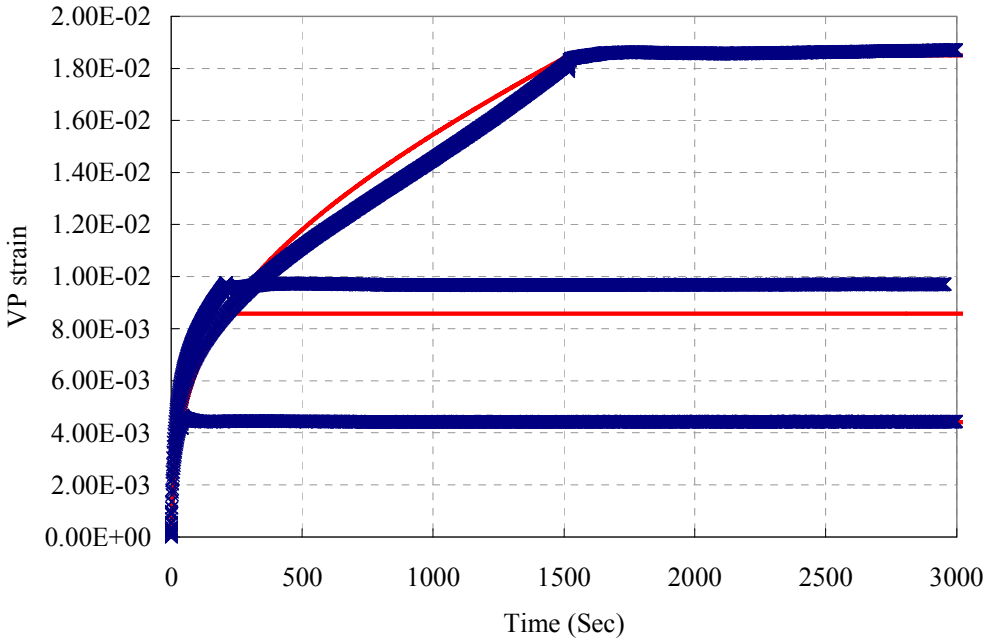

(a)

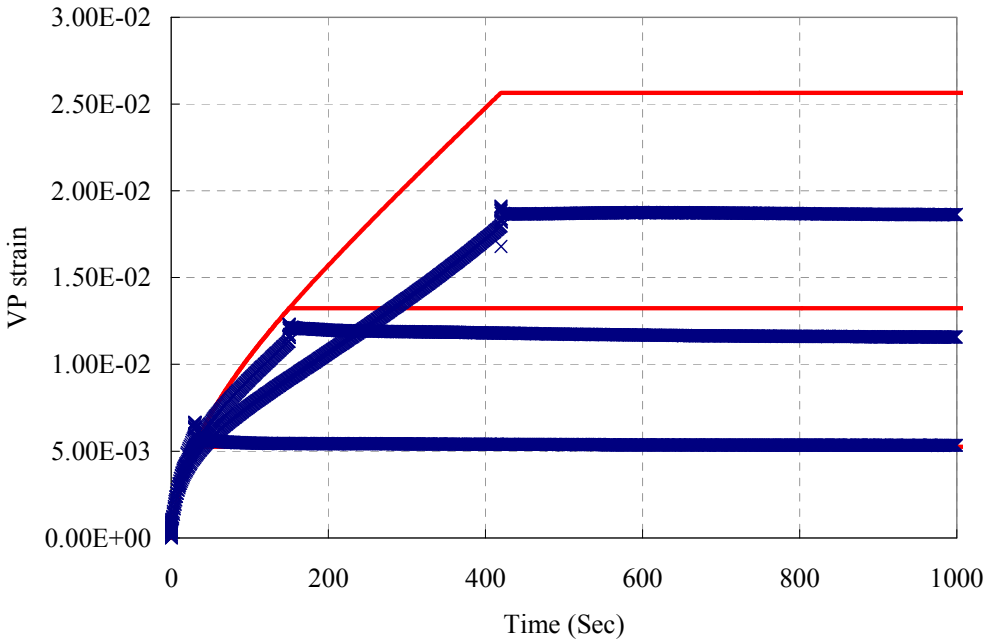

(b)

Figure 21. The comparison of viscoplastic strain between measurements and model predictions at temperature 20^{o}C for stress levels: (a) 1000 kPa and (b) 1500 kPa.

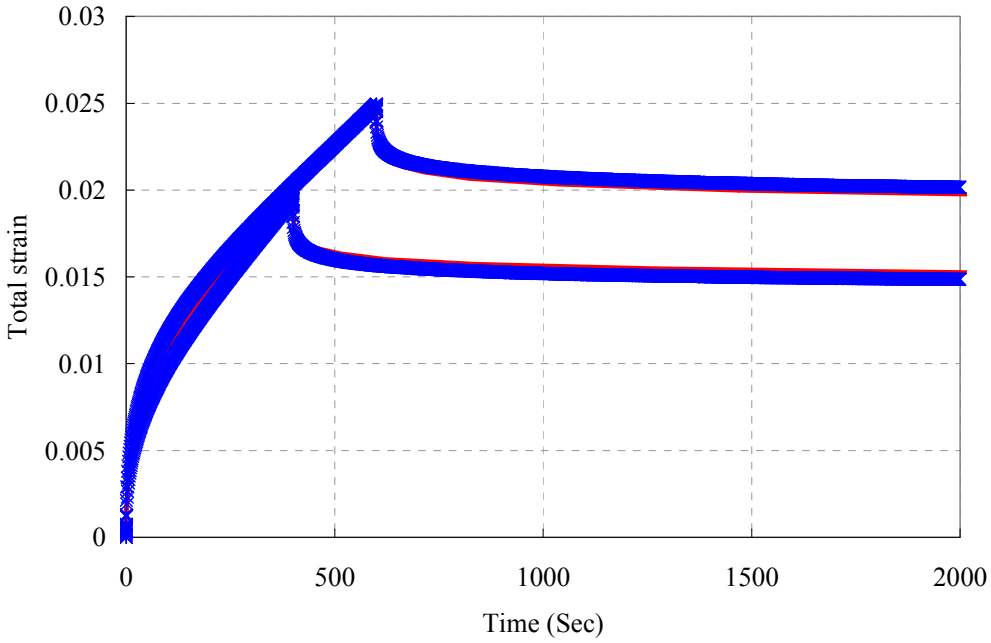

(a)

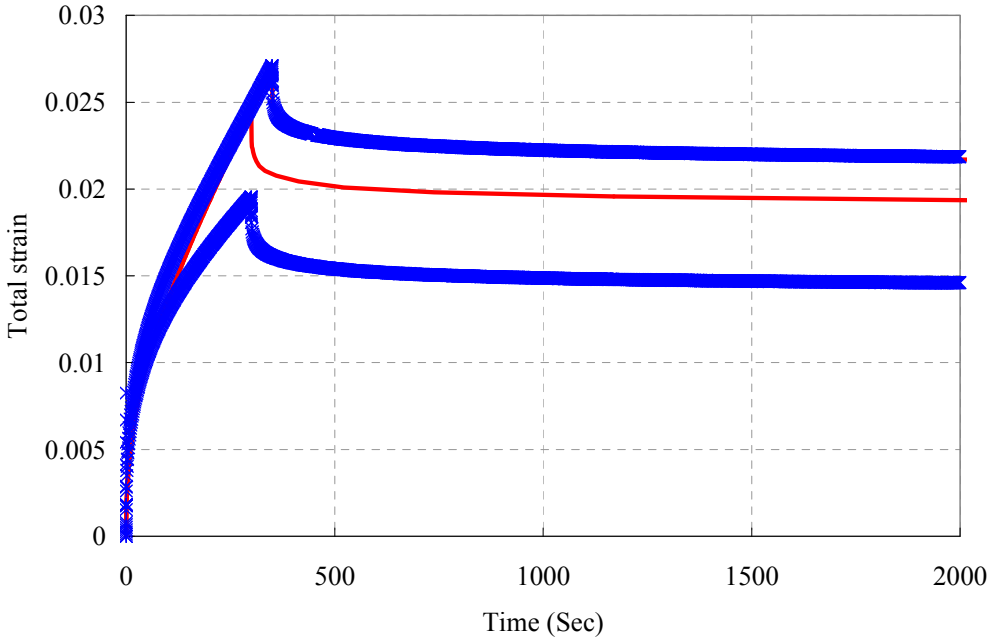

(b)

Figure 22. The comparison of total strain between measurements and model predictions at temperature 10^{o}C for stress levels: (a) 2000 kPa and (b) 2500 kPa.

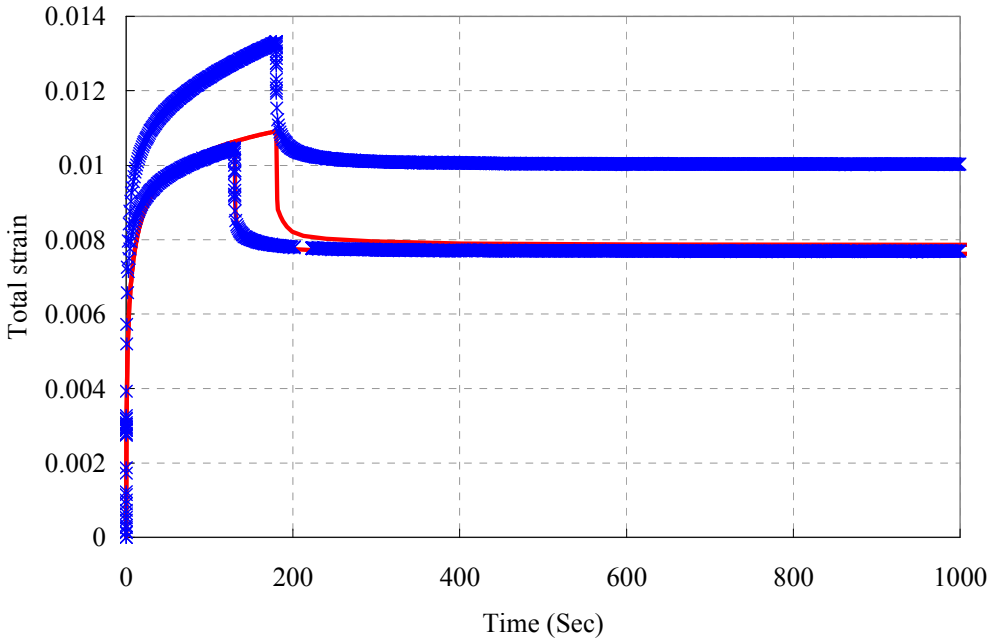

(a)

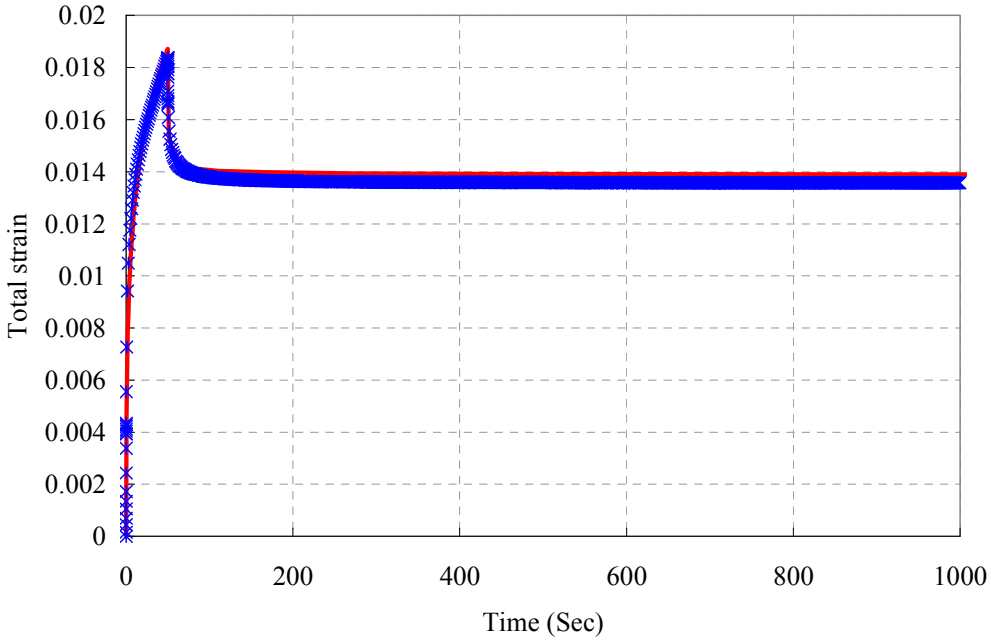

(b)

Figure 23. The comparison of total strain between measurements and model predictions at temperature 40^{o}C for stress levels: (a) 500 kPa and (b) 750 kPa.

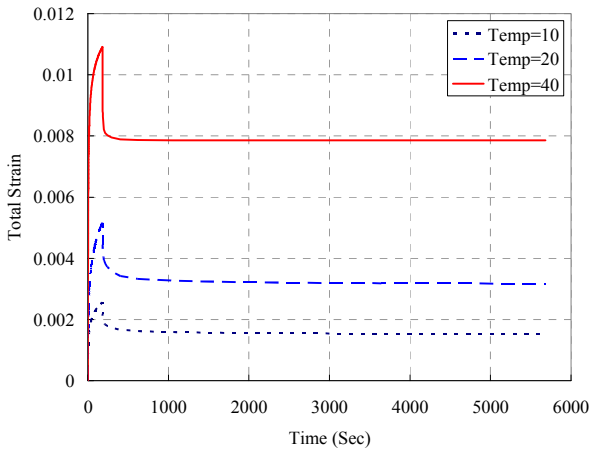

(a)

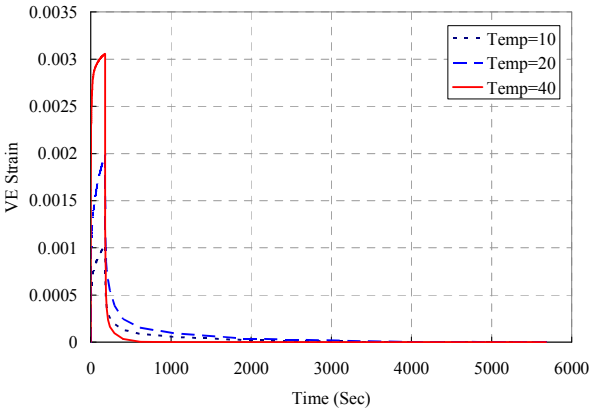

(b)

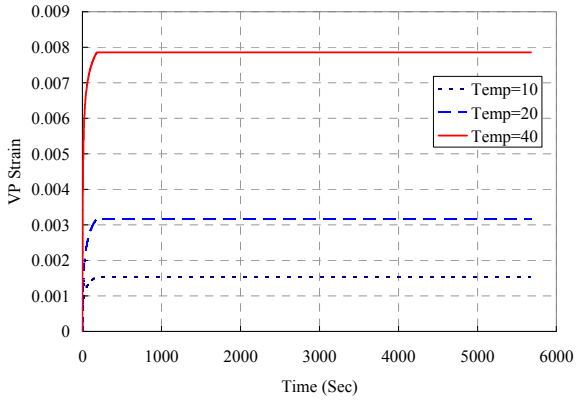

(c)

Figure 24. The comparison of material response at different temperature (in ^{o}C) for: (a) total strain, (b) viscoelastic strain, and (c) viscoplastic strain.

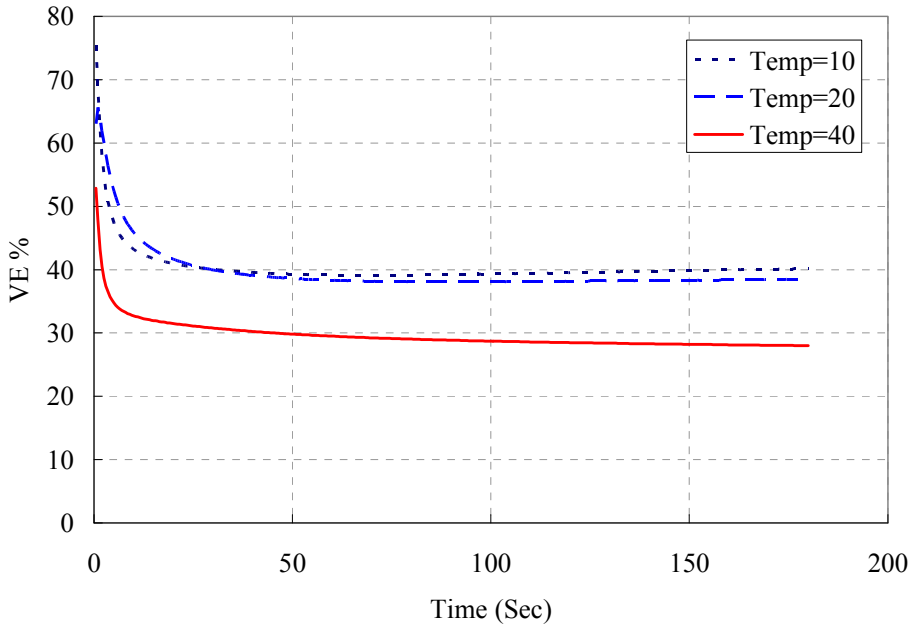

(a)

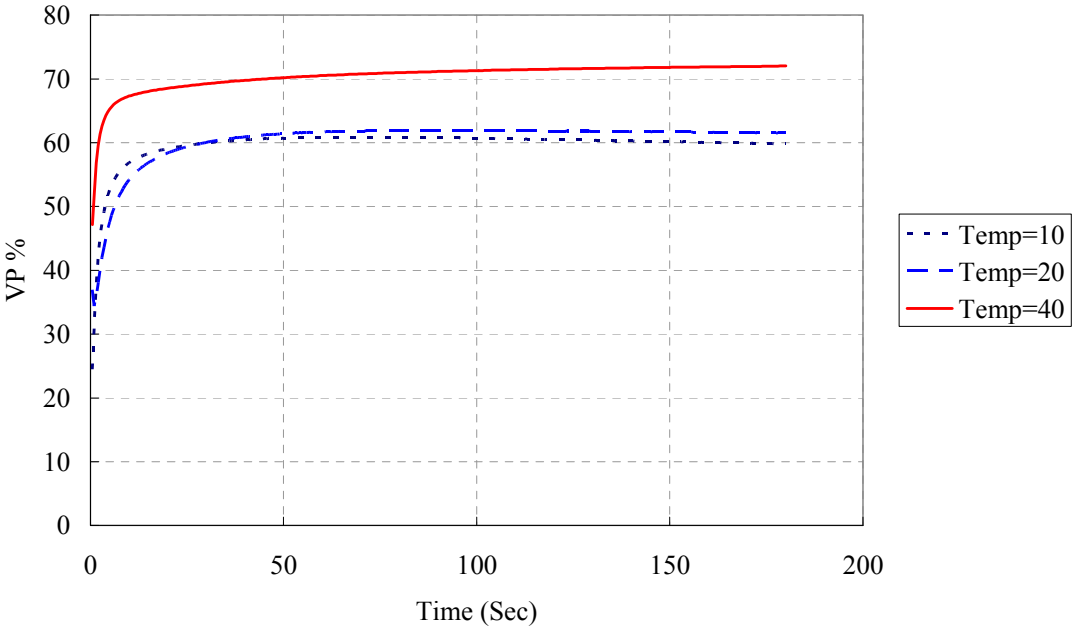

(b)

Figure 25. The comparison at different temperatures (in ^{o}C) for: (a) the viscoelastic strain percentage and (b) the viscoplastic strain percentage.

5 Conclusions

The focus of this study is on the coupling of nonlinear viscoelasticity and viscoplasticity for modeling the nonlinear behavior of asphalt concrete mixes. The computational algorithm necessary to enhance this coupling is developed and validated against a set of creep-recovery experimental data for different constant stress levels and different temperatures. A systematic calibration procedure is proposed for identifying the material parameters associated with the nonlinear viscoelastic model and the viscoplastic model. The results from the experimental analysis show that the viscoelastic strain component exhibits a nonlinear response, which justifies the need for a nonlinear viscoelastic model, particularly, at high stress levels and temperatures. The viscoplastic parameters are identified by separating the viscoelastic and viscoplastic strain components. The viscoplastic analysis indicated that the overstress function in Perzyna model should be modified by normalizing it with respect to the stress in order to incorporate the applied stress effect on the viscoplastic yield surface. The analysis also shows that the viscosity parameter Γ increases with increasing temperature, whereas the viscoplasticity isotropic hardening parameters decrease with decreasing temperature. In fact, the experimental analyses indicate that a viscoplastic model different than the Perzyna viscoplasticity could be necessary to model the viscoplastic response of asphaltic mixes.

The constitutive model is validated by comparing the finite element results with experimental measurements at different combinations of temperatures and stress levels, and the results show that the model predictions have good agreements with the experimental measurements. Moreover, the numerical simulations at different temperatures show that increasing the temperature will increase the percentage of the viscoplastic strain, but decrease the percentage of the viscoelastic strain from the total strain. This result indicated that the viscoelastic response controls the material behavior at lower temperatures, and the viscoplastic response dominates the material behavior at higher temperatures. Moreover, the presented results illustrate that the model can explain the material behavior at different temperatures, different stress levels, and different loading times.

The present analysis only considers the creep-recovery test and it is, therefore, needed to analyze more different tests in order to fully validate the present constitutive model such as the triaxial test and the uniaxial constant strain rate test in order to obtain the viscoplastic properties individually. Moreover, the lowest stress level at each temperature, which is used in this study

for identifying the material constants associated with linear viscoelasticity, could have induced a nonlinear viscoelastic behavior. Therefore, it is needed to conduct the test at small stress levels and temperatures in order to accurately identify the linear viscoelastic material parameters. Also, future work will focus on coupling the presented nonlinear viscoelastic and viscoplastic model with a continuum damage mechanics framework.

References

ABAQUS (2008). *Version 6.8*, Habbit, Karlsson and Sorensen, Inc, Providence, RI.

Airey, G., Rahimzadeh, B., Collop, A.C. (2002a). "Linear viscoelastic limits of bituminous binders." *Journal of Associated Asphalt Paving Technologists*, 17, 89–115.

Airey, G., Rahimzadeh, B., Collop, A.C. (2002b). "Viscoelastic linearity limits for bituminous materials." *Materials and Structures*, 36(10), 643–647.

Airey, G., Rahimzadeh, B., Collop, A.C. (2004). "Linear rheological behavior of bituminous paving material." *Journal of Materials in Civil Engineering*, 16, 212–220.

Chen W. F. and Han D. J. (1988). *Plasticity for structural engineers*, Springer-Verlag, New York.

Cheung, C., Cebon, D. (1997). "Deformation mechanisms of pure bitumen." *Journal of Materials in Civil Engineering*, 9, 117–129.

Christensen, R.M. (1968). "On obtaining solutions in nonlinear viscoelasticity." *Journal of Applied Mechanics*, 35, 129–133.

Collop, A.C., Scarpas, A. T., Kasbergen, C., and de Bondt, A. (2003). "Development and finite element implementation of stress-dependent elastoviscoplastic constitutive model with damage for asphalt." *Transportation Research Record 1832*, Transportation Research Board, Washington, DC, 96-104.

Dessouky, S., (2005). "Multiscale approach for modeling hot mix asphalt." Ph.D. dissertation, Texas A&M University, College Station, TX.

Grenfell, J. R. A., Collop, A. C., Airey, G.D., Taherkhani, H. and Scarpas A. (2009). "Deformation characterization of asphalt concrete behaviour." *Journal of the Association of Asphalt Paving Technologists*, (In press).

Haj-Ali, R.M. and Muliana, A.H. (2004). "Numerical finite element formulation of the Schapery non-linear viscoelastic material model." *International Journal for Numerical Methods in Engineering*, 59, 25–45.

Huang, C.W., Masad, E., Muliana, A., and Bahia, H. (2007). "Nonlinear viscoelastic analysis of asphalt mixes subjected to shear loading." *Mechanics of Time Dependent Materials*, 11, 91-110.

Kim, Y. Allen, D. H., and Little D. N., (2007). "Computational constitutive model for predicting nonlinear viscoelastic damage and fracture failure of asphalt concrete mixtures." *International Journal of Geomechanics*, 7, 102-110.

Kose, S., Guler, M., Bahia, H., and Masad, E. (2000). "Distribution of strains within hot-mix asphalt binders." *Transportation Research Record 1728*, Transportation Research Board, Washington, DC, 21–27.

Lai, J. and Bakker, A. (1996) "3D schapery representation of non-linear viscoelasticity and finite element implementation," *Computational Mechanics*, 18, 182-191.

Lee, H. J. and Kim, Y. R. (1998). "A uniaxial viscoelastic constitutive model for asphalt concrete under cyclic loading." *Journal of Engineering Mechanics*, 124, 32-40.

Lemaitre, J. and Chaboche, J.-L. (1990). *Mechanics of Solid Materials*, Cambridge University Press, London.

Lu, Y. and Wright, P. J. (1998). "Numerical approach of visco-elastoplastic analysis for asphalt mixtures." *Journal of Computers and Structures*, 69, 139-157.

Masad, E., and Somadevan, N. (2002). "Microstructural finite-element analysis of influence of localized strain distribution of asphalt mix properties." *Journal of Engineering Mechanics*, 128, 1105–1114.

Masad, E., Tashman, L., Little D., and Zbib, H. (2005). "Viscoplastic modeling of asphalt mixes with the effects of anisotropy, damage, and aggregate characteristics." *Journal of Mechanics of Materials*, 37, 1242-1256.

Masad, E., Dessouky, S., and Little, D. (2007). "Development of an elastoviscoplastic microstructural-based continuum model to predict permanent deformation in hot mix asphalt." *International Journal of Geomechanics*, 7, 119-130.

Perl, M. Uzan, J., and Sides, A. (1983). "Visco-elasto-plastic constitutive law for bituminous mixture under repeated loading." *Transportation Research Record 911*, Transportation Research Board, Washington, DC, 20-26.

Perzyna, P. (1971) "Thermodynamic theory of viscoplastcity," *Advances in Applied Mechanics*, 11, 313-354.

Saadeh, S., Masad, E., and Little, D. (2007). "Characterization of hot mix asphalt using anisotropic damage viscoelastic-viscoplastic model and repeated loading." *Journal of Materials in Civil Engineering*, 19 (10), 912-924.

Sadd, M.H., Parameswaran, D.Q., and Shukla, A. (2004). "Simulation of asphalt materials using finite element micromechanical model with damage mechanics." *Transportation Research Record 1832*, Transportation Research Board, Washington, DC, 86–95.

Schapery, R.A. (1969). "On the characterization of nonlinear viscoelastic materials." *Polymer Engineering and Science*, 9, 295–310.

Schapery, R. A. (1991). "Simplifications in the behavior of viscoelastic composites with growing damage." In Proc., IUTAM Symposium on Inelastic Deformation of Composite Materials, Springer Verlag, Berlin.

Schapery, R.A. (2000). "Nonlinear viscoelastic solids." *International Journal of Solids and Structures*, 37, 359–366.

Seibi, A. C., Sharma, M. G., Ali, G. A., and Kenis, W. J. (2001). "Constitutive relations for asphalt concrete under high rates of loading." *Transportation Research Record 1767*, Transportation Research Board, Washington, DC, 111-119.

Sides, A., Uzan, J., and Perl, M. (1985). "A comprehensive visco-elastoplastic characterization of sand-asphalt under compression and tension cyclic loading." *Journal of Testing and Evaluation*, 13, 49-59.

Tashman, L. Masad E., Zbib, H., Little D., and Kaloush, K. (2005). "Microstructural viscoplastic continuum model for asphalt pavements." *Journal of Engineering Mechanic*, 131 (1), 48-57.

Touati, D., and Cederbaum, G. (1998). "Post buckling of nonlinear viscoelastic imperfect laminated plates, Part I: Material considerations." *Composite Structures*, 42, 33–41.

Wang, W.M., Sluys, L.J., de Borst, R. (1997). "Viscoplasticity for instabilities due to strain softening and strain-rate softening," *Int. J. Numer. Meth. Engng.*, 40, 3839-3864.